QCD equation of state to $\mathcal{O}(\mu_B^6)$ from lattice QCD

A. Bazavov,[1] H.-T. Ding,[2] P. Hegde,[3,*] O. Kaczmarek,[2,4] F. Karsch,[4,5] E. Laermann,[4] Y. Maezawa,[6] Swagato Mukherjee,[5] H. Ohno,[5,7] P. Petreczky,[5] H. Sandmeyer,[4] P. Steinbrecher,[4,5] C. Schmidt,[4] S. Sharma,[5] W. Soeldner,[8] and M. Wagner[9]

[1]*Department of Computational Mathematics, Science and Engineering and Department of Physics and Astronomy, Michigan State University, East Lansing, Michigan 48824, USA*
[2]*Key Laboratory of Quark & Lepton Physics (MOE) and Institute of Particle Physics, Central China Normal University, Wuhan 430079, China*
[3]*Center for High Energy Physics, Indian Institute of Science, Bangalore 560012, India*
[4]*Fakultät für Physik, Universität Bielefeld, D-33615 Bielefeld, Germany*
[5]*Physics Department, Brookhaven National Laboratory, Upton, New York 11973, USA*
[6]*Yukawa Institute for Theoretical Physics, Kyoto University, Kyoto 606-8317, Japan*
[7]*Center for Computational Sciences, University of Tsukuba, Tsukuba, Ibaraki 305-8577, Japan*
[8]*Institut für Theoretische Physik, Universität Regensburg, D-93040 Regensburg, Germany*
[9]*NVIDIA GmbH, D-52146 Würselen, Germany*

(Received 20 January 2017; published 7 March 2017)

We calculated the QCD equation of state using Taylor expansions that include contributions from up to sixth order in the baryon, strangeness and electric charge chemical potentials. Calculations have been performed with the Highly Improved Staggered Quark action in the temperature range $T \in [135\ \mathrm{MeV}, 330\ \mathrm{MeV}]$ using up to four different sets of lattice cutoffs corresponding to lattices of size $N_\sigma^3 \times N_\tau$ with aspect ratio $N_\sigma/N_\tau = 4$ and $N_\tau = 6-16$. The strange quark mass is tuned to its physical value, and we use two strange to light quark mass ratios $m_s/m_l = 20$ and 27, which in the continuum limit correspond to a pion mass of about 160 and 140 MeV, respectively. Sixth-order results for Taylor expansion coefficients are used to estimate truncation errors of the fourth-order expansion. We show that truncation errors are small for baryon chemical potentials less then twice the temperature ($\mu_B \leq 2T$). The fourth-order equation of state thus is suitable for the modeling of dense matter created in heavy ion collisions with center-of-mass energies down to $\sqrt{s_{NN}} \sim 12$ GeV. We provide a parametrization of basic thermodynamic quantities that can be readily used in hydrodynamic simulation codes. The results on up to sixth-order expansion coefficients of bulk thermodynamics are used for the calculation of lines of constant pressure, energy and entropy densities in the T-μ_B plane and are compared with the crossover line for the QCD chiral transition as well as with experimental results on freeze-out parameters in heavy ion collisions. These coefficients also provide estimates for the location of a possible critical point. We argue that results on sixth-order expansion coefficients disfavor the existence of a critical point in the QCD phase diagram for $\mu_B/T \leq 2$ and $T/T_c(\mu_B = 0) > 0.9$.

DOI: 10.1103/PhysRevD.95.054504

I. INTRODUCTION

The temperature and density dependence of bulk thermodynamic quantities, commonly summarized as the equation of state (EoS), provide the most basic characterization of equilibrium properties of strong-interaction matter. Its analysis within the framework of lattice regularized Quantum Chromodynamics (QCD) has been refined ever since the early calculations performed in pure $SU(N)$ gauge theories [1]. Quite recently, the continuum extrapolated results for the EoS of QCD with physical light and strange quark masses have been calculated [2,3]. Bulk thermodynamic observables such as pressure (P), energy density (ϵ) and entropy density (s) as well as second-order quantities such as the specific heat (C_V) and velocity of sound (c_s) have now been obtained at vanishing chemical potentials for the three quark flavors (μ_u, μ_d, μ_s). In accordance with the analysis of the chiral transition temperature, $T_c \simeq (154 \pm 9)$ MeV [4], bulk thermodynamic observables change smoothly in the transition region. At low temperature they are found to be in quite good agreement with hadron resonance gas (HRG) model calculations, although some systematic deviations have been observed, which may be attributed to the existence of additional resonances which are not taken into account in HRG model calculations based on well established resonances listed in the particle data tables [5,6].

The EoS at vanishing chemical potentials does already provide important input into the modeling of the hydrodynamic evolution of hot and dense matter created in heavy ion collisions. While this is appropriate for the thermal conditions met in these collisions at the LHC and the

*Correspondence author.
prasad@chep.iisc.ernet.in

highest RHIC beam energies, knowledge of the EoS at nonvanishing baryon (μ_B), strangeness (μ_S) and electric charge (μ_Q) chemical potentials is indispensable for the hydrodynamic modeling of the conditions met in the beam energy scan (BES) at RHIC. Due to the well-known sign problem for lattice QCD formulations at nonzero chemical potential, a direct calculation of the EoS at nonzero (μ_B, μ_Q, μ_S) is unfortunately not yet possible. At least for small values of the chemical potentials this can be circumvented by using a Taylor expansion of the thermodynamic potential [7,8]. In this way some results for EoS at nonzero baryon chemical potential have been obtained on coarse lattices [8–10]. These calculations have even been extended to sixth order in the baryon chemical potential [11,12]. First continuum extrapolated results for the EoS using second-order Taylor expansion coefficients have been obtained within the stout discretization scheme for staggered fermions [13], and simulations at imaginary chemical potential have been used to arrive at a sixth-order result for the QCD EoS [14] and up to eighth order for some generalized susceptibilities [15] through analytic continuation.

Results for higher-order expansion coefficients are clearly needed if one wants to cover the range of chemical potentials, $0 \leq \mu_B/T \lesssim 3$ that is expected to be explored with the BES at RHIC by varying the beam energies in the range 7.7 GeV $\leq \sqrt{s_{NN}} \leq 200$ GeV. Of course, the Taylor expansions will break down, should the elusive critical point in the QCD phase diagram [16,17] turn out to be present in this range of baryon chemical potentials. The convergence of the series thus needs to be monitored carefully.

This paper is organized as follows. In the next section we briefly discuss Taylor series for a HRG model in Boltzmann approximation. This helps to argue for the significance of sixth-order Taylor expansions. In Sec. III we present the basic framework of Taylor series expansions, introduce expansions in the presence of global constraints and discuss some details of our calculations and the ensembles used. In Sec. IV we discuss the sixth-order Taylor expansion of QCD thermodynamics in the simplified case of vanishing strangeness and electric charge chemical potentials. Section V is devoted to the corresponding discussion of strangeness neutral systems $n_S = 0$ with fixed net electric charge (n_Q) to net baryon-number (n_B) ratio, which is of relevance for the description of hot and dense matter formed in heavy ion collisions where typically $n_Q/n_B \simeq 0.4$. We discuss the relevance of a nonvanishing electric charge chemical potential by considering electric charge neutral ($n_Q/n_B = 0$) as well as isospin symmetric ($n_Q/n_B = 1/2$) systems. At the end of this section we present a parametrization of the equation of state that can easily be used as input for the modeling of the thermal conditions met in heavy ion collisions. In Sec. VI we present results on lines of constant pressure, energy density and entropy density and compare their dependence on μ_B with empirical results for the freeze-out conditions observed in heavy ion collisions. We comment on the radius of convergence of the Taylor series for the pressure and resulting constraints for the location of a possible critical point in Sec. VII. Finally, we present our conclusions in Sec. VIII. Details on (A) the statistics and simulation parameters, (B) explicit expressions for the expansions of electric charge and baryon number chemical potentials, and (C) explicit expressions for the expansion parameters of the lines of constant physics are given in the three Appendices A–C.

II. TAYLOR EXPANSIONS AND THE LOW AND HIGH TEMPERATURE LIMITS OF STRONG INTERACTION MATTER

The main aim of this work is to supply an EoS of strong-interaction matter using up to sixth-order Taylor expansions for bulk thermodynamic observables. As we see later, present results on sixth-order expansion coefficients in the Taylor series mainly help to constrain truncation errors in the fourth-order expansion rather than providing accurate results on the sixth-order contribution to thermodynamic quantities. We argue that our analysis provides reliable results for the EoS for baryon chemical potentials up to $\mu_B/T \simeq 2$ at temperatures below $T \simeq 160$ MeV and for an even larger range in μ_B/T at higher temperatures.

Before turning to a discussion of lattice QCD results on the EoS, it may be useful to analyze truncation effects in the hadron resonance gas (HRG) model, which seems to provide a good approximation for thermodynamics in the low temperature, hadronic regime. For simplicity, let us consider the case of vanishing electric charge and strangeness chemical potentials, $\mu_Q = \mu_S = 0$. At temperatures close to the transition temperature $T_c \simeq 154$ MeV and for baryon chemical potentials less than a few times the transition temperature, the baryon sector of a HRG is well described in the Boltzmann approximation. In a HRG model calculation based on noninteracting hadrons, the pressure may then be written as

$$\begin{aligned} P(T,\mu_B) &= P_M(T) + P_B(T,\hat{\mu}_B) \\ &= P_M(T) + P_B(T,0) + P_B(T,0)(\cosh(\hat{\mu}_B) - 1), \end{aligned} \tag{1}$$

where we introduced the notation $\hat{\mu}_B \equiv \mu_B/T$ and $P_M(T)$ ($P_B(T,\hat{\mu}_B)$) denotes the meson (baryon) contributions to the pressure. A similar relation holds for the energy density,

$$\begin{aligned} \epsilon(T,\mu_B) &= \epsilon_M(T) + \epsilon_B(T,\hat{\mu}_B) \\ &= \epsilon_M(T) + \epsilon_B(T,0) + \epsilon_B(T,0)(\cosh(\hat{\mu}_B) - 1), \end{aligned} \tag{2}$$

with $\epsilon_{M/B} \equiv T^2(\partial(P_{M/B}/T)/\partial T)_{\hat{\mu}_B}$. The μ_B-dependent contribution thus is simple and can easily be represented by a Taylor series. Truncating this expansion at $(2n)$th order we obtain

$$(\Delta(P/T^4))_{2n} \equiv \frac{(P_B(T,\mu_B) - P_B(T,0))_{2n}}{T^4} = \sum_{k=1}^{n} \frac{\chi_{2k}^{B,HRG}(T)}{(2k)!}\hat{\mu}_B^{2k} \simeq \frac{P_B(T,0)}{T^4}\sum_{k=1}^{n}\frac{1}{(2k)!}\hat{\mu}_B^{2k}, \quad (3)$$

where in the last equality we made use of the fact that in HRG models constructed from noninteracting, pointlike hadrons, all expansion coefficients are identical when using a Boltzmann approximation for the baryon sector; i.e. all baryon number susceptibilities are identical, $\chi_{2k}^{B,HRG} = P_B(T,0)$. The ratios of these susceptibilities are unity, $\chi_{2k}^{B,HRG}/\chi_{2(k-1)}^{B,HRG} = \chi_{2k}^{B,HRG}/\chi_2^{B,HRG} = 1$. Similarly one finds for the net baryon-number density,

$$\frac{n_B}{T^3} = \frac{P_B(T,0)}{T^4}\sinh\hat{\mu}_B = \sum_{k=1}^{\infty}\frac{\chi_{2k}^{B,HRG}(T)}{(2k-1)!}\hat{\mu}_B^{2k-1} \simeq \frac{P_B(T,0)}{T^4}\sum_{k=1}^{\infty}\frac{1}{(2k-1)!}\hat{\mu}_B^{2k-1}. \quad (4)$$

Higher-order corrections are thus more important in the net baryon-number density than in the expansions of the pressure or energy density. For instance, the contribution to $\mu_B n_B/T^4$ at $\mathcal{O}(\hat{\mu}_B^{2k})$ is a factor $2k$ larger than the corresponding $\mathcal{O}(\hat{\mu}_B^{2k})$ expansion coefficient of the pressure.

In Fig. 1 we show results from a Taylor series expansion of the μ_B-dependent part of the pressure in a HRG model truncated after leading order (LO), next-to-leading order (NLO) and next-to-next-to-leading (NNLO) order. These truncated expansions are compared to the exact result; i.e. $(\Delta P)_\infty(T) = P_B(T)(\cosh(\hat{\mu}_B) - 1)$. The insertion shows the deviation of the nth order truncated Taylor series ($(\Delta P)_n(T)$) from the exact result ($(\Delta P)_\infty(T)$). As can be seen already, the fourth-order Taylor series provides a good approximation for the pressure (and energy as well as entropy density) of a HRG for all $\mu_B \leq 2T$. At $\mu_B = 2T$, the fourth-order Taylor series for the μ_B-dependent contribution to the pressure deviates by less than 5% from the exact result. These deviations are, of course, even smaller in the total pressure which in the temperature range of interest is dominated by the meson contribution. Even at $T = 170$ MeV, which certainly is already above the range of applicability of HRG models, the baryonic contribution to the pressure (energy density) amounts only to about 20% (30%). A 5% truncation error in the μ_B-dependent contribution to the pressure or energy density thus amounts to less than a 2% effect in the total pressure or energy density. Similar estimates hold for the more general case of nonvanishing μ_Q and μ_S.

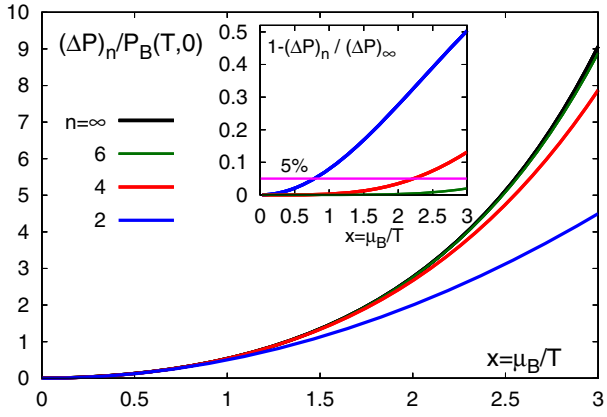

FIG. 1. The nth order Taylor series, $(\Delta P)_n$ for $(\Delta P)_\infty = P_B(T,0)(\cosh(x) - 1)$ compared to the exact result. The insertion shows the relative error due to truncation of the Taylor series after nth order. Note that the sixth-order result is hardly visible behind the exact result.

Of course, the good convergence properties of the Taylor series for the pressure in HRG models also reflect that the radius of convergence of this series is infinite. If there exists a critical point in the QCD phase diagram, one cannot expect to find that the Taylor series is that well behaved. Still the HRG result provides a benchmark also for the QCD case. If the radius of convergence of the Taylor series for the QCD pressure is finite and, in particular, smaller than $\mu_B \simeq 3T$, one should find large deviations in the generalized susceptibilities from the corresponding HRG results. Ratios of susceptibilities have to grow asymptotically like $\chi_{2k}^{B,QCD}/\chi_{2(k-1)}^{B,QCD} \sim k^2$ in order to yield a finite radius of convergence for a Taylor expansion. We come back to a discussion of this asymptotic behavior after having discussed our sixth-order calculation of Taylor expansion coefficients.

Let us briefly mention also the high temperature limit. At large values of the temperature, the pressure approaches that of a massless ideal gas of quarks and gluons. In this limit the pressure is just a second order polynomial in $\hat{\mu}_f^2$,

$$\frac{P_{\text{ideal}}}{T^4} = \frac{8\pi^2}{45} + \sum_{f=u,d,s}\left[\frac{7\pi^2}{60} + \frac{1}{2}\left(\frac{\mu_f}{T}\right)^2 + \frac{1}{4\pi^2}\left(\frac{\mu_f}{T}\right)^4\right], \quad (5)$$

In this limit a fourth-order Taylor expansion thus provides the exact results for the basic bulk thermodynamic observables. This also is correct in leading order perturbation theory, i.e. at $\mathcal{O}(g^2)$ [18].

III. OUTLINE OF THE CALCULATION

A. Taylor series in baryon number, electric charge and strangeness chemical potentials

Our goal is the calculation of Taylor expansion coefficients for basic bulk thermodynamic observables of

strong-interaction matter in terms of chemical potentials μ_X for conserved charges ($X = B, Q, S$). We start with the expansion of the pressure, P, in terms of the dimensionless ratios $\hat{\mu}_X \equiv \mu_X/T$, which are the logarithms of fugacities,

$$\frac{P}{T^4} = \frac{1}{VT^3}\ln \mathcal{Z}(T, V, \hat{\mu}_u, \hat{\mu}_d, \hat{\mu}_s) = \sum_{i,j,k=0}^{\infty} \frac{\chi^{BQS}_{ijk}}{i!j!k!}\hat{\mu}_B^i \hat{\mu}_Q^j \hat{\mu}_S^k, \tag{6}$$

with $\chi^{BQS}_{000} \equiv P(T,0)/T^4$. The chemical potentials for conserved charges are related to the quark chemical potentials (μ_u, μ_d, μ_s),

$$\begin{aligned} \mu_u &= \frac{1}{3}\mu_B + \frac{2}{3}\mu_Q, \\ \mu_d &= \frac{1}{3}\mu_B - \frac{1}{3}\mu_Q, \\ \mu_s &= \frac{1}{3}\mu_B - \frac{1}{3}\mu_Q - \mu_S. \end{aligned} \tag{7}$$

The expansion coefficients χ^{BQS}_{ijk}, i.e. the so-called generalized susceptibilities, can be calculated at vanishing chemical potential,[1]

$$\chi^{BQS}_{ijk} \equiv \chi^{BQS}_{ijk}(T) = \left.\frac{\partial P(T,\hat{\mu})/T^4}{\partial \hat{\mu}_B^i \partial \hat{\mu}_Q^j \partial \hat{\mu}_S^k}\right|_{\hat{\mu}=0}. \tag{8}$$

From Eq. (6) it is straightforward to obtain the Taylor series for the number densities,

$$\frac{n_X}{T^3} = \frac{\partial P/T^4}{\partial \hat{\mu}_X}, \qquad X = B, Q, S. \tag{9}$$

This only requires knowledge of the expansion coefficients entering the series for P/T^4. The energy (ϵ) and entropy (s) densities, on the other hand, also require derivatives of the generalized susceptibilities with respect to temperature, which are the expansion coefficients of the trace anomaly,

$$\Delta(T, \hat{\mu}_B, \hat{\mu}_Q, \hat{\mu}_S) \equiv \frac{\epsilon - 3P}{T^4} = T\frac{\partial P/T^4}{\partial T} = \sum_{i,j,k=0}^{\infty} \frac{\Xi^{BQS}_{ijk}}{i!j!k!}\hat{\mu}_B^i \hat{\mu}_Q^j \hat{\mu}_S^k, \tag{10}$$

with $i + j + k$ even and

$$\Xi^{BQS}_{ijk}(T) = T\frac{\mathrm{d}\chi^{BQS}_{ijk}(T)}{\mathrm{d}T}. \tag{11}$$

With this one finds for the Taylor expansions of the energy and entropy densities,

$$\frac{\epsilon}{T^4} = \sum_{i,j,k=0}^{\infty} \frac{\Xi^{BQS}_{ijk} + 3\chi^{BQS}_{ijk}}{i!j!k!}\hat{\mu}_B^i \hat{\mu}_Q^j \hat{\mu}_S^k, \tag{12}$$

$$\frac{s}{T^3} = \frac{\epsilon + p - \mu_B n_B - \mu_Q n_Q - \mu_S n_S}{T^4} = \sum_{i,j,k=0}^{\infty} \frac{\Xi^{BQS}_{ijk} + (4 - i - j - k)\chi^{BQS}_{ijk}}{i!j!k!}\hat{\mu}_B^i \hat{\mu}_Q^j \hat{\mu}_S^k. \tag{13}$$

B. Constrained series expansions

In our calculations we generated all generalized susceptibilities up to sixth order, which are needed to set up the general Taylor series in terms of the three conserved charge chemical potentials as discussed in the previous subsection. In the following we, however, consider only thermodynamic systems, in which the electric charge and strangeness chemical potentials are fixed by additional constraints and become functions of the baryon chemical potential and temperature. We only consider constraints that can be fulfilled order by order in the Taylor series expansion. That is, for the construction of the sixth-order Taylor series of the pressure in terms of $\hat{\mu}_B$ we need to know the expansion of $\hat{\mu}_Q(T, \mu_B)$ and $\hat{\mu}_S(T, \mu_B)$ up to fifth order in $\hat{\mu}_B$,

$$\begin{aligned} \hat{\mu}_Q(T, \mu_B) &= q_1(T)\hat{\mu}_B + q_3(T)\hat{\mu}_B^3 + q_5(T)\hat{\mu}_B^5 + \ldots, \\ \hat{\mu}_S(T, \mu_B) &= s_1(T)\hat{\mu}_B + s_3(T)\hat{\mu}_B^3 + s_5(T)\hat{\mu}_B^5 + \ldots. \end{aligned} \tag{14}$$

The above parametrization includes the cases of vanishing electric charge and strangeness chemical potentials, $\mu_Q = \mu_S = 0$, which we are going to discuss in the next section as well as the strangeness neutral case with fixed electric charge to baryon-number ratio, which we analyze in Sec. V.

Implementing the constraints specified in Eq. (14) in the Taylor series for the pressure and net conserved-charge number densities, one obtains series in terms of the baryon chemical potential only,

$$\frac{P(T,\mu_B)}{T^4} - \frac{P(T,0)}{T^4} = \sum_{k=1}^{\infty} P_{2k}(T)\hat{\mu}_B^{2k}, \tag{15}$$

$$\frac{n_X}{T^3} = \sum_{k=1}^{\infty} N^X_{2k-1}\hat{\mu}_B^{2k-1}, \qquad X = B, Q, S. \tag{16}$$

Using

[1]We often suppress the argument (T) of the generalized susceptibilities. We also suppress superscripts and subscripts of χ^{BQS}_{ijk} whenever one of the subscripts vanishes, e.g. $\chi^{BQS}_{i0k} \equiv \chi^{BS}_{ik}$.

$$\hat{\mu}_B \frac{\mathrm{d}P/T^4}{\mathrm{d}\hat{\mu}_B} = \hat{\mu}_B \frac{n_B}{T^3} + \hat{\mu}_B \frac{\mathrm{d}\hat{\mu}_Q}{\mathrm{d}\hat{\mu}_B}\frac{n_Q}{T^3} + \hat{\mu}_B \frac{\mathrm{d}\hat{\mu}_S}{\mathrm{d}\hat{\mu}_B}\frac{n_S}{T^3}, \quad (17)$$

and the series expansions of $\hat{\mu}_Q$ and $\hat{\mu}_S$ given in Eq. (14) one easily finds the relation between the expansion coefficients for the pressure and number densities,

$$P_{2n} = \frac{1}{2n}\left(N^B_{2n-1} + \sum_{k=1}^{n}(2k-1)(s_{2k-1}N^S_{2n-2k+1} + q_{2k-1}N^Q_{2n-2k+1})\right). \quad (18)$$

When imposing constraints on the electric charge and strangeness chemical potentials, these generally become temperature-dependent functions as indicated in Eq. (14). The temperature derivative of P/T^4 at fixed $\hat{\mu}_B$ in the constraint case and the partial derivative of P/T^4 at fixed $(\hat{\mu}_B, \hat{\mu}_Q, \hat{\mu}_S)$, which defines the trace anomaly Δ [Eq. (10)], thus are related through

$$T\frac{\mathrm{d}P/T^4}{\mathrm{d}T} = \Delta + T\hat{\mu}'_Q\frac{n_Q}{T^3} + T\hat{\mu}'_S\frac{n_S}{T^3}, \quad (19)$$

where the (total) temperature derivative $\mathrm{d}/\mathrm{d}T$ is taken at fixed $\hat{\mu}_B$ and $\hat{\mu}'_X = \mathrm{d}\hat{\mu}_X/\mathrm{d}T$. With this we obtain the Taylor series for the trace anomaly,

$$\Delta(T,\hat{\mu}_B) = \frac{\epsilon - 3P}{T^4} = \left(\frac{\epsilon-3P}{T^4}\right)_{\hat{\mu}_B=0} + \sum_{n=1}^{\infty}(TP'_{2n}(T) - h_{2n}(T))\hat{\mu}_B^{2n}, \quad (20)$$

with

$$h_{2n} = \sum_{k=1}^{n}(s'_{2k-1}N^S_{2n-2k+1} + q'_{2k-1}N^Q_{2n-2k+1}). \quad (21)$$

We also introduce

$$t_{2n} = \sum_{k=1}^{n}(s_{2k-1}N^S_{2n-2k+1} + q_{2k-1}N^Q_{2n-2k+1}). \quad (22)$$

With this the Taylor series expansion of the energy and entropy densities for constraint cases, in which $\hat{\mu}_Q$ and $\hat{\mu}_S$ satisfy Eq. (14), becomes

$$\frac{\epsilon(T,\mu_B)}{T^4} - \frac{\epsilon(T,0)}{T^4} = \sum_{n=1}^{\infty}\epsilon_{2n}(T)\hat{\mu}_B^{2n}, \quad (23)$$

$$\frac{s(T,\mu_B)}{T^3} - \frac{s(T,0)}{T^3} = \sum_{n=1}^{\infty}\sigma_{2n}(T)\hat{\mu}_B^{2n}, \quad (24)$$

with $\epsilon_{2n}(T) = 3P_{2n}(T) + TP'_{2n}(T) - h_{2n}(T)$ and $\sigma_{2k}(t) = 4P_{2n}(T) + TP'_{2n}(T) - N^B_{2n-1}(T) - h_{2n}(T) - t_{2n}(T)$.

C. Numerical calculation of generalized susceptibilities up to $\mathcal{O}(\mu^6)$

The generalized susceptibilities χ^{BQS}_{ijk} have been calculated on gauge field configurations generated for $(2+1)$-flavor QCD using the Highly Improved Staggered Quark (HISQ) action [19] and the tree-level improved Symanzik gauge action.

All calculations are performed using a strange quark mass m_s tuned to its physical value. We performed calculations with two different light to strange quark mass ratios, $m_l/m_s = 1/27$ and $1/20$. The former corresponds to a pseudoscalar Goldstone mass, which in the continuum limit yields a pion mass $m_\pi \simeq 140$ MeV, the latter leads to a pion mass $m_\pi \simeq 160$ MeV. These parameters are fixed using the line of constant physics determined by HotQCD from the f_K scale. Using $f_K = 155.7(9)/\sqrt{2}$ MeV allows us to determine the lattice spacing $a(\beta)$ at a given value of the gauge coupling β and the corresponding set of quark masses (m_l, m_s), which in turn fixes the temperature on a lattice with temporal extent N_τ; i.e. $T = (N_\tau a)^{-1}$. More details on the scale determination are given in [4].

All calculations have been performed on lattices of size $N_\sigma^3 N_\tau$ with an aspect ratio $N_\sigma/N_\tau = 4$. We perform calculations in the temperature interval $T \in [135\ \mathrm{MeV}, 330\ \mathrm{MeV}]$ using lattices with temporal extent $N_\tau = 6, 8, 12$ and 16, which corresponds to four different values of the lattice spacings at fixed temperature. At temperatures $T \leq 175$ MeV all calculations have been performed with the lighter, physical quark mass ratio $m_l/m_s = 1/27$. In the high temperature region quark mass effects are small, and we based our calculations on existing data sets for $m_l/m_s = 1/20$, which have previously been generated by the HotQCD Collaboration and used for the calculation of second-order susceptibilities [20]. These data sets have been extended for the calculation of higher-order susceptibilities. Gauge field configurations are stored after every tenth molecular dynamics trajectory of unit length.

All calculations of fourth- and sixth-order expansion coefficients have been performed on lattices with temporal extent $N_\tau = 6$ and 8. In these cases we gathered a large amount of statistics. At low temperatures we have generated up to 1.2 million trajectories for $N_\tau = 6$ and up to 1.8 million trajectories for $N_\tau = 8$. At high temperature less than a tenth of this statistic turned out to be sufficient. The second-order expansion coefficients have been calculated on lattices with four different temporal extends, $N_\tau = 6$, 8, 12, 16. At fixed temperature this corresponds to four different values of the lattice cutoff, which we used to extract continuum extrapolated results for the second-order expansion coefficients. We also extrapolated results for the higher-order expansion coefficients to the continuum limit.

However, having at hand results from only two lattice spacings for these expansion coefficients, we consider these extrapolations as estimates of the results in the continuum limit.

On each configuration the traces of all operators needed to construct up to sixth-order Taylor expansion coefficients have been calculated stochastically. For the calculation of second- and fourth-order expansion coefficients, we follow the standard approach of introducing a nonzero chemical potential in the QCD Lagrangian as an exponential prefactor for timelike gauge field variables [21]; i.e. the chemical potential μ_f for quark flavor f is introduced through a factor $e^{\mu_f a}$ ($e^{-\mu_f a}$) on timelike links directed in the forward (backward) direction. This insures that all observables calculated are free of ultraviolet divergences. For the calculation of all sixth-order expansion coefficients, we use the so-called linear-μ approach [22,23]. This becomes possible as no ultraviolet divergences appear in sixth-order cumulants and above. In the linear-μ formulation the number of operators that contribute to cumulants is drastically reduced, and their structure is simplified. All operators appearing in the exponential formulation, that involve second- or higher-order derivatives of the fermion matrix [11], vanish. The remaining operators are identical in both formulations. One thus only has to calculate traces of observables that are of the form,

$$\mathrm{Tr} M_f^{-1} M_f' M_f^{-1} M_f' \ldots . M_f^{-1} M_f',$$

where M_f is the staggered fermion matrix for light ($f = l$) or strange ($f = s$) quarks, respectively, and M_f' denotes its derivative with respect to the flavor chemical potential $\hat{\mu}_f$. The final error on these traces depends on the noise due to the use of stochastic estimators for the inversion of the fermion matrices M_f, as well as on the gauge noise resulting from a finite set of gauge configurations that get analyzed. We analyzed the signal to noise ratio for all traces of operators that we calculate and identified the operator $D_1 = M_f^{-1} M_f'$ as being particularly sensitive to the stochastic noise contribution. This operator has been measured using 2000 random noise vectors. For the calculation of traces of all other operators, we used 500 random noise vectors. We checked that this suffices to reduce the stochastic noise well below the gauge noise. The simulation parameters and the statistics accumulated in this calculation are summarized in the tables of Appendix A.

All fits and continuum extrapolations shown in the following are based on spline interpolations with coefficients that are allowed to depend quadratically on the inverse temporal lattice size. Our fitting ansatz and the strategy followed to arrive at continuum extrapolated results are described in detail in Ref. [3]. For the current analysis we found it sufficient to use spline interpolations with quartic polynomials and three knots whose location is allowed to vary in the fit range.

IV. EQUATION OF STATE FOR $\mu_Q = \mu_S = 0$

Let us first discuss the Taylor expansion for bulk thermodynamic observables in the case of vanishing electric charge and strangeness chemical potentials. This greatly simplifies the discussion and yet incorporates all the features of the more general case. Also the discussion of truncation errors presented in this section carries over to the more general situation.

A. Pressure and net baryon-number density

For $\mu_Q = \mu_S = 0$, the Taylor expansion coefficients P_{2n} and N^B_{2n-1}, introduced in Eqs. (15) and (16), are simply related by

$$P_{2n} = \frac{1}{2n} N^B_{2n-1} = \frac{1}{(2n)!} \chi^B_{2n}. \tag{25}$$

The series for the pressure and net baryon-number density simplify to

$$\begin{aligned} \frac{P(T,\mu_B) - P(T,0)}{T^4} &= \sum_{n=1}^{\infty} \frac{\chi^B_{2n}(T)}{(2n)!} \left(\frac{\mu_B}{T}\right)^{2n} \\ &= \frac{1}{2}\chi^B_2(T)\hat{\mu}_B^2 \left(1 + \frac{1}{12}\frac{\chi^B_4(T)}{\chi^B_2(T)}\hat{\mu}_B^2 + \frac{1}{360}\frac{\chi^B_6(T)}{\chi^B_2(T)}\hat{\mu}_B^4 + \cdots\right), \end{aligned} \tag{26}$$

$$\begin{aligned} \frac{n_B}{T^3} &= \sum_{n=1}^{\infty} \frac{\chi^B_{2n}(T)}{(2n-1)!} \hat{\mu}_B^{2n-1} \\ &= \chi^B_2(T)\hat{\mu}_B \left(1 + \frac{1}{6}\frac{\chi^B_4(T)}{\chi^B_2(T)}\hat{\mu}_B^2 + \frac{1}{120}\frac{\chi^B_6(T)}{\chi^B_2(T)}\hat{\mu}_B^4 + \cdots\right). \end{aligned} \tag{27}$$

In Eqs. (26) and (27) we have factored out the leading order (LO) μ_B-dependent part in the series for the pressure as well as the net baryon-number density. This helps to develop a feeling for the importance of higher-order contributions and, in particular, the approach to the HRG limit at low temperatures. Note that all ratios χ^B_{2n}/χ^B_2 are unity in a HRG, and in the infinite temperature, ideal quark gas limit, $\chi^B_4/\chi^B_2 = 2/(3\pi^2) \simeq 0.068$ is the only nonvanishing higher-order expansion coefficient. From Eqs. (26) and (27), it is evident that contributions from higher-order expansion coefficients become more important in the number density than in the pressure. Relative to the LO result, the contributions of the NLO and NNLO expansion coefficients for n_B/T^3 are a factor two and three larger, respectively, than for the corresponding expansion coefficients in the pressure series.

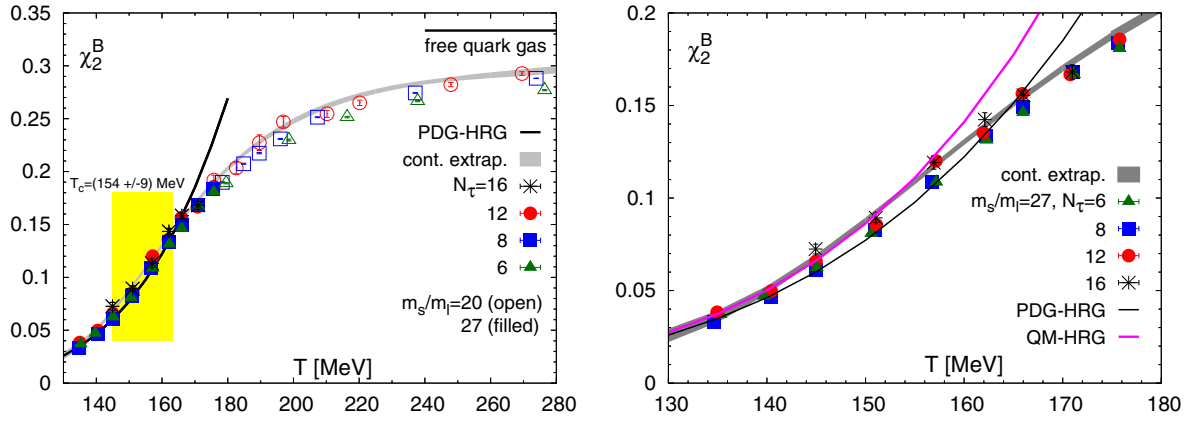

FIG. 2. The leading order ($\mathcal{O}(\mu_B^2)$) correction to the pressure calculated at zero baryon chemical potential. The left-hand figure shows the leading order correction in a large temperature range. The right-hand part of the figure shows an enlarged view into the low temperature region. In addition to the continuum extrapolation of the lattice QCD results, we also show results from HRG model calculations based on all hadron resonances listed by the particle data group (PDG-HRG) and obtained in quark model calculations (QM-PDG).

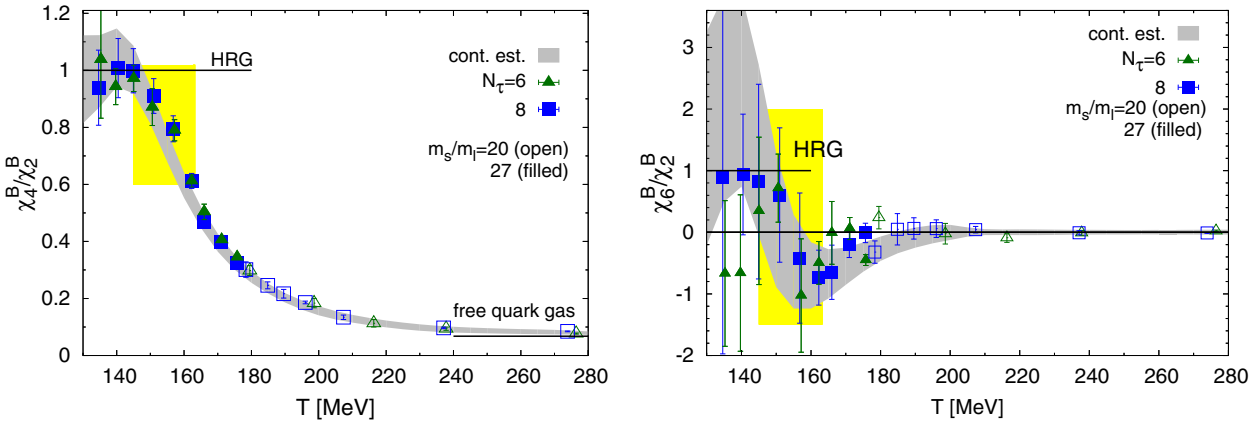

FIG. 3. (Left) The ratio of fourth- and second-order cumulants of net-baryon number fluctuations (χ_4^B/χ_2^B) versus temperature. (Right) Same as the left-hand side, but for the ratio of sixth- and second-order cumulants of net-baryon number fluctuations (χ_6^B/χ_2^B). The boxes indicate the transition region, $T_c = (154 \pm 9)$ MeV. Grey bands show continuum estimate.

We show the leading order coefficient $\chi_2^B(T)$ in Fig. 2 and the NLO (χ_4^B) and NNLO (χ_6^B) coefficients divided by $\chi_2^B(T)$ in Fig. 3. The left-hand part of Fig. 2 shows the leading order contribution χ_2^B in the entire temperature interval used in the current analysis. For the LO expansion coefficients, we also used data from simulations on $48^3 \times 12$ lattices. Here, we used existing data for $m_l/m_s = 1/20$ [3] and generated new ensembles for $m_l/m_s = 1/27$ at nine temperature values below $T = 175$ MeV. Furthermore, we used data on $64^3 \times 16$ lattices at a corresponding set of low temperature values. These data are taken from an ongoing calculation of higher-order susceptibilities performed by the HotQCD Collaboration.[2] This allowed us to update the continuum extrapolation for χ_2^B given in [20]. The new continuum extrapolation shown in Fig. 2 is consistent with our earlier results, but has significantly smaller errors in the low temperature region. In the right-hand part of this figure we compare the continuum extrapolated lattice QCD data for χ_2^B with HRG model calculations. It is obvious that the continuum-extrapolated QCD results overshoot results obtained from a conventional, noninteracting HRG model calculations with resonances taken from the particle data tables (PDG-HRG) and treated as pointlike excitations. We therefore compare the QCD results also with a HRG model that includes additional strange baryons, which are not listed in the PDG but are predicted in quark models and lattice QCD calculations. We successfully used such an extended HRG model (QM-HRG) in previous calculations [5,6]. As can be seen in Fig. 2 (left), continuum extrapolated results for χ_2^B agree well with QM-HRG calculations.

As can be seen in the left-hand part of Fig. 3, the ratio χ_4^B/χ_2^B approaches unity with decreasing temperature, but is small at high temperatures where the leading order correction is large. The relative contribution of the NLO correction thus is largest in the hadronic phase, where $\chi_4^B/\chi_2^B \simeq 1$. For temperatures $T \lesssim 155$ MeV, we find

[2]We thank the HotQCD Collaboration for providing access to the second-order quark number susceptibilities.

$\chi_4^B/\chi_2^B \leq 0.8$. The relative contribution of the NLO correction to the μ_B-dependent part of the pressure (number density) in the crossover region and below thus is about 8% (16%) at $\mu_B/T = 1$ and rises to about 33% (66%) at $\mu_B/T = 2$. At temperatures larger than 180 MeV, the relative contribution of the NLO correction to pressure and number density at $\mu_B/T = 2$ is less than 8% and 16%, respectively.

The relative contribution of the $\mathcal{O}(\hat{\mu}_B^6)$ correction, χ_6^B/χ_2^B, is shown in the right-hand part of Fig. 3. The ideal gas limit for this ratio vanishes. Obviously the ratio is already small for all temperatures $T > 180$ MeV; i.e. $\chi_6^B/\chi_2^B \leq 0.5$. Consequently, for $\hat{\mu}_B = 2$, the correction to the leading order result is less than 2.2% for the μ_B-dependent part of the pressure and less than 7% for the net baryon-number density. At lower temperatures, the statistical errors on current results for χ_6^B/χ_2^B are still large. However, a crude estimate for the magnitude of this ratio at all temperatures larger than 130 MeV suggests $|\chi_6^B/\chi_2^B| \leq 3$. In the low temperature, hadronic regime and for $\hat{\mu}_B = 2$ the $\mathcal{O}(\hat{\mu}_B^6)$ corrections to the μ_B-dependent part of the pressure can be about 13%. However, in the total pressure, which also receives large contributions from the meson sector, this will result only in an error of less than 3%. In the calculation of the net baryon-number density, on the other hand, the current uncertainty on $\mathcal{O}(\hat{\mu}_B^6)$ expansion coefficients results in errors of about 40% at temperatures below $T \simeq 155$ MeV. In fact, as discussed already in Sec. II, higher-order corrections are larger in the Taylor expansion of the number density. From Eq. (25), it follows for the ratio of NLO and LO expansion coefficients, $N_5^B/N_1^B = 3P_6/P_2$. Clearly, better statistics are needed in the low temperature range to control higher-order corrections to n_B/T^3.

In Fig. 4 we show results for the μ_B-dependent part of the pressure (left) and the net baryon-number density (right) calculated from Taylor series up to and including LO, NLO and NNLO contributions, respectively. This suggests that up to $\mu_B \simeq 2T$ results for the pressure at low temperature are well described by a Taylor series truncated at NNLO, while at higher temperature NNLO corrections are small even at $\mu_B \simeq 3T$. This also is the case for n_B/T^3, although the NNLO correction is large at low temperatures and, at present, does not allow for a detailed quantitative analysis of the baryon-number density in this temperature range.

It also is obvious that the Taylor series for the pressure and n_B/T^3 in the temperature range up to $T \simeq 180$ MeV are sensitive to the negative contributions of the sixth-order expansion coefficient. The occurrence of a dip in the sixth-order expansion coefficient of the pressure has been expected to show up on the basis of general scaling arguments for higher order derivatives of the QCD pressure in the vicinity of the chiral phase transition [24]. It may, however, also reflect the influence of a singularity on the imaginary chemical potential axis [25] (Roberge-Weiss critical point [26]) on Taylor series of bulk thermodynamic observables in QCD. Even with improved statistics, it thus is expected that the wiggles, that start to show up in the expansion of pressure and net baryon-number density above $\mu_B/T \simeq 2$ (see Fig. 4) and reflect the change of sign in the sixth-order expansion coefficient, will persist. Getting the magnitude of the dip in χ_6^B/χ_2^B at $T \simeq 160$ MeV under control in future calculations thus is of importance for the understanding of this nonperturbative regime of the QCD equation of state in the high temperature phase close to the transition region. This also indicates that higher-order corrections need to be calculated in order to control the equation of state in this temperature regime.

B. Net strangeness and net electric charge densities

For vanishing strangeness and electric charge chemical potentials, the corresponding net strangeness (n_S) and net

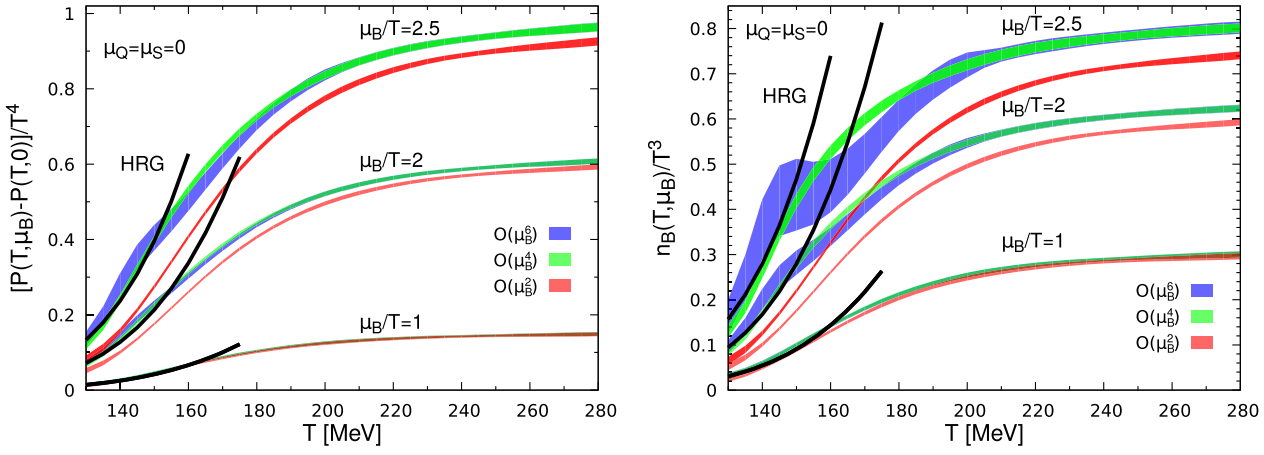

FIG. 4. The μ_B-dependent contribution to the pressure (left) and the baryon-number density (right) in the case of vanishing electric charge and strangeness chemicals potential for several values of the baryon chemical potential in units of temperature. The different bands show results including Taylor series results up to the order indicated.

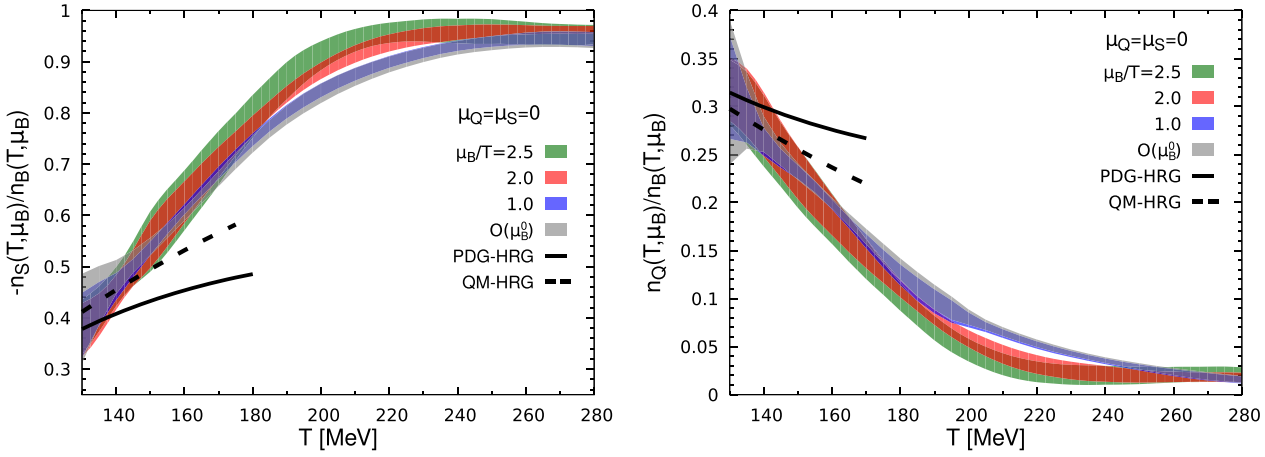

FIG. 5. The ratio of net strangeness and net baryon-number densities (left) and the ratio of net electric charge and net baryon-number densities (right). At low temperatures, results from hadron resonance gas calculations at $\mu_B = 0$ are shown (see text).

electric charge (n_Q) densities are nonetheless nonzero because the carriers of these quantum numbers also carry baryon number. The ratios of number densities are given by

$$\frac{n_X}{n_B} = \frac{\chi_{11}^{BX} + \frac{1}{6}\chi_{31}^{BX}\hat{\mu}_B^2 + \frac{1}{120}\chi_{51}^{BX}\hat{\mu}_B^4}{\chi_2^B + \frac{1}{6}\chi_4^B\hat{\mu}_B^2 + \frac{1}{120}\chi_6^B\hat{\mu}_B^4}, \qquad X = Q, S. \tag{28}$$

In a hadron resonance gas the ratios n_S/n_B and n_Q/n_B are independent of the baryon chemical potential, and irrespective of the value of $\hat{\mu}_B$, these ratios approach -1 and 0, respectively, in the $T \to \infty$ limit. One thus may expect that these ratios only show a mild dependence on $\hat{\mu}_B$, which indeed is apparent from the results of the NNLO expansions shown in Fig. 5.

For $\mu_Q = \mu_S = 0$, nonvanishing electric charge and strangeness densities only arise due to a nonzero baryon-chemical potential. In the low temperature HRG phase n_Q and n_S thus only receive contributions from charged baryons or strange baryons, respectively. The ratios n_Q/n_B and n_S/n_B thus are sensitive to the particle content in a hadron resonance gas, and a comparison with PDG-HRG and QM-HRG is particularly sensitive to the differences in the baryon content in these two models. It is apparent from Fig. 5 that at low temperatures the QM-HRG model provides a better description of the lattice QCD results than the PDG-HRG model.

C. The energy and entropy densities

In order to calculate the energy and entropy densities, defined in Eqs. (23) and (24), we need to extract the temperature derivative of the expansion coefficients of the pressure. We use as a starting point the representation of the pressure given in Eq. (26) and calculate the temperature derivatives of χ_n^B from the splines used to fit this observable. With this, we construct the expansion coefficients $\epsilon_n^B(T)$ and σ_n^B defined in Eqs. (12) and (13),

$$\Delta(\epsilon/T^4) = \frac{\epsilon(T,\mu_B) - \epsilon(T,0)}{T^4} = \sum_{k=1}^{3} \epsilon_{2k}\hat{\mu}_B^{2k} = \sum_{k=1}^{3} (TP'_{2k} + 3P_{2k})\hat{\mu}_B^{2k}, \tag{29}$$

$$\Delta(s/T^3) = \frac{s(T,\mu_B) - s(T,0)}{T^3} = \sum_{k=1}^{3} \sigma_{2k}\hat{\mu}_B^{2k} = \sum_{k=1}^{3} (\epsilon_{2k} - (2k-1)P_{2k})\hat{\mu}_B^{2k}. \tag{30}$$

We show the LO and NLO expansion coefficients for energy and entropy densities together with the expansion coefficient for the pressure in Fig. 6. Because of Eq. (25), the expansion coefficients of the net baryon-number density are simply proportional to those of the pressure.

Clearly, the temperature dependence of the expansion coefficients of the energy and entropy densities shows more structure than in the case of the pressure. Qualitatively, this can be understood in terms of the pseudocritical behavior of bulk thermodynamic observables. Once thermodynamic quantities are dominated by contributions from the singular part of the free energy, which is expected to happen in the transition region, they become functions of $(T - T_c) + \kappa\hat{\mu}_B^2$. The temperature derivative of the expansion coefficient P_2, which gives ϵ_2, thus will show properties similar to those of P_4. The LO correction ϵ_2^B/T^4 has a mild peak, which results from the strongly peaked T-derivative of χ_2^B which is qualitatively similar to χ_4^B, and the NLO correction is negative in a small temperature interval above T_c, which arises from the negative T-derivative of χ_4^B at high temperature, which resembles the negative part of χ_6^B at high temperature.

Although the temperature dependence of ϵ_n and σ_n differs from that of the pressure coefficient, P_n, the conclusions drawn for the relative strength of the expansion coefficients

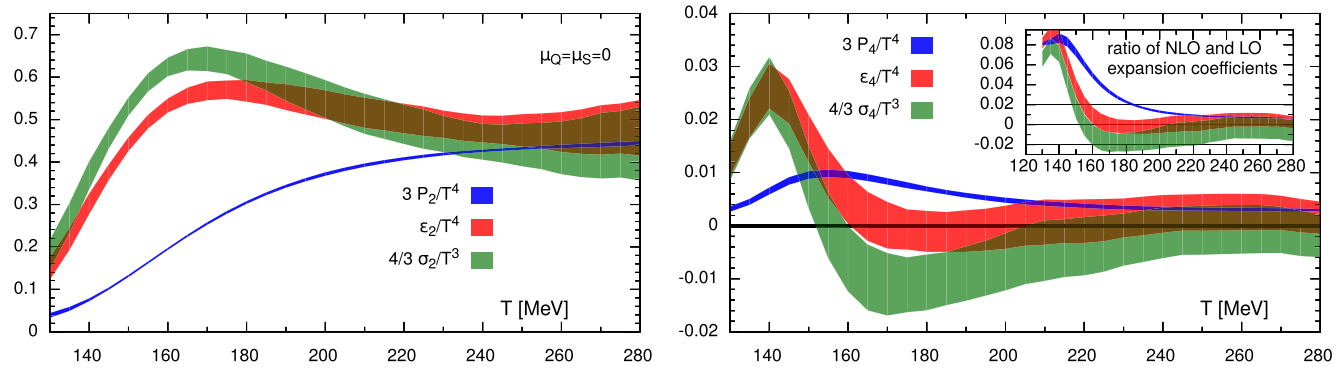

FIG. 6. Leading order (left) and next-to-leading order (right) expansion coefficients for the μ_B-dependent part of pressure, the energy and entropy densities in the case $\mu_Q = \mu_S = 0$. The inset in the right-hand figure shows the ratios of NLO and LO expansion coefficients P_4/P_2, ϵ_4/ϵ_2 and σ_4/σ_2. Note that the expansion coefficients for the net baryon-number density are directly proportional to those of the pressure series; i.e. $N_1^B = 2P_2$ and $N_3^B = 4P_4$.

are identical in all cases. As can be seen from the inset in Fig. 6 (right), the relative contribution of the NLO expansion coefficients never exceeds 10%. In particular, at temperatures larger than 180 MeV, the magnitude of the NLO expansion coefficients never exceeds 2% of the LO expansion coefficients. Again this leads to the conclusion that at $\mu_B/T = 2$ and temperatures above 180 MeV the NLO correction contributes less than 8% of the leading correction to μ_B-dependent part of the energy and entropy densities. For $T \lesssim 155$ MeV, however, the NLO contribution can rise to about 30%. A similar conclusion holds for the $\mathcal{O}(\hat{\mu}_B^6)$ corrections, although it requires higher statistics to better quantify the magnitude of this contribution. In Fig. 7 we show results for the total pressure and total energy density. For P/T^4 and ϵ/T^4 at $\mu_B = 0$, we used the results obtained by the HotQCD Collaboration [3] and added to it the results from the $\mathcal{O}(\hat{\mu}_B^6)$ expansions presented above. This figure also makes it clear that despite of the large error of higher-order expansion coefficients, which we have discussed above, the error on the total pressure and energy density still is dominated by errors on their values at $\mu_B = 0$.

V. EQUATION OF STATE IN STRANGENESS NEUTRAL SYSTEMS

A. Taylor expansion of pressure, baryon-number, energy and entropy densities

We now discuss the equation of state for strangeness neutral systems with a fixed ratio of electric charge to baryon-number density; i.e. we impose the constraints [27]

$$n_S = 0, \qquad \frac{n_Q}{n_B} = r. \tag{31}$$

These constraints can be realized through suitable choices of the electric charge and strangeness chemical potentials. This thus is a particular case of the constraint expansion discussed in Sec. III B. The expansion coefficients q_n, s_n, $n = 1, 3, 5$ needed to satisfy these constraints are given in Appendix B. For $r = 0.4$, the constrained EoS obtained in this way is usually considered to be most appropriate for applications to heavy ion collisions. We do, however, in the following also comment on other choices of r, including the case of isospin symmetric systems ($r = 1/2$) and electric charge neutral matter ($r = 0$).

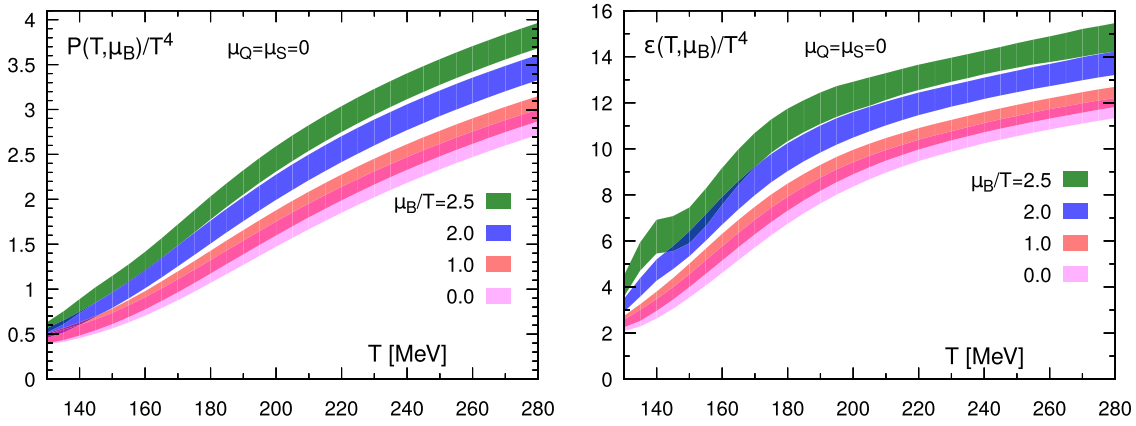

FIG. 7. (Left) The total pressure in $(2+1)$-flavor QCD in $\mathcal{O}(\hat{\mu}_B^6)$ for several values of μ_B/T. (Right) The total energy density in $(2+1)$-flavor QCD in $\mathcal{O}(\hat{\mu}_B^6)$ for several values of μ_B/T. The results for $\hat{\mu}_B = 0$ are taken from Ref. [3].

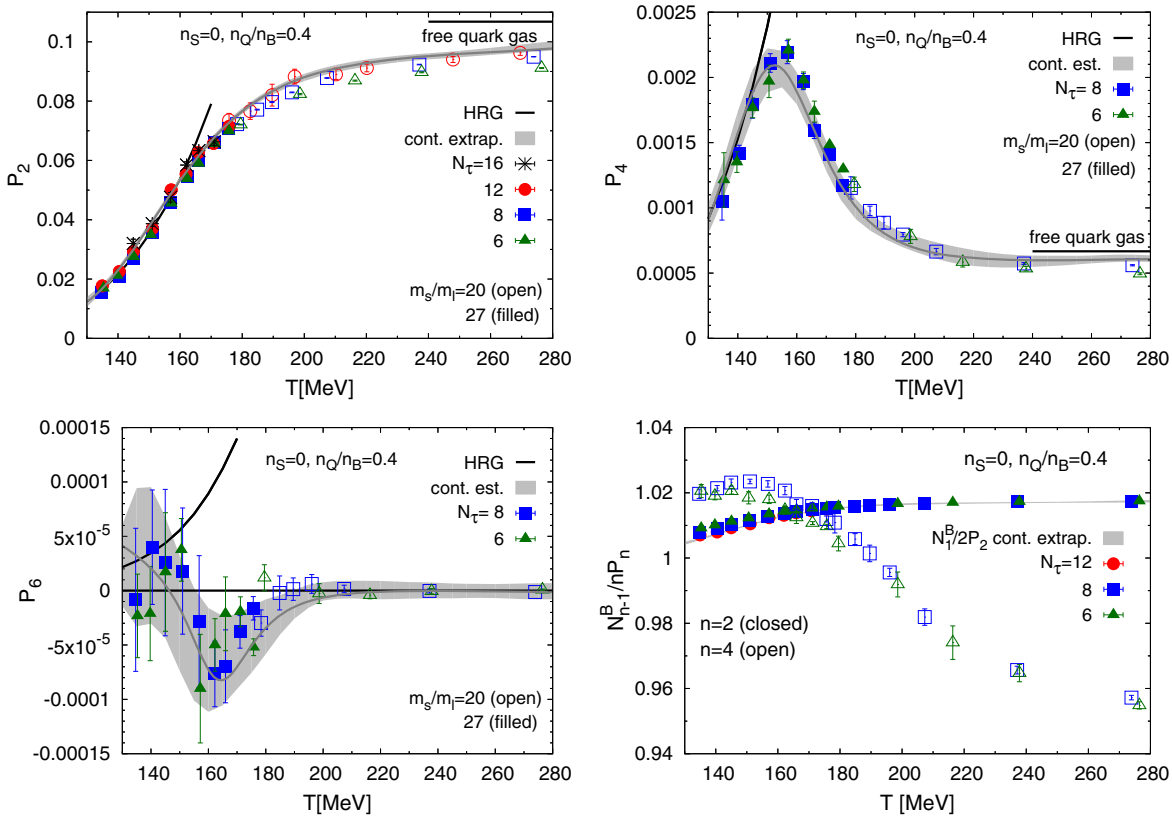

FIG. 8. Expansion coefficients of the pressure (top and bottom left) and the ratio of net baryon-number density and pressure expansion coefficients (bottom right) in strangeness neutral systems with $r = 0.4$. Broad bands show continuum extrapolations as discussed in Sec. III. The darker lines in the center of the error bands of these extrapolations show the interpolating fits discussed in Sec. V B. At low temperature, lines for HRG model calculations based on hadron resonances listed by the Particle Data Group are shown.

Using the constraints specified in Eq. (31) and the definition of the pressure in terms of generalized susceptibilities, χ^{BQS}_{ijk}, the expansion coefficients P_{2n} can easily be determined. Here, it advantageous to use the relation between the Taylor expansion coefficients of the pressure, P_{2n}, and number densities, N^X_{2n-1}, given in Eq. (18), which simplifies considerably for strangeness neutral systems. It now involves only the net baryon-number density coefficients,

$$P_2 = \frac{1}{2}[N_1^B + rq_1N_1^B], \tag{32}$$

$$P_4 = \frac{1}{4}[N_3^B + r(q_1N_3^B + 3q_3N_1^B)], \tag{33}$$

$$P_6 = \frac{1}{6}[N_5^B + r(q_1N_5^B + 3q_3N_3^B + 5q_5N_1^B)]. \tag{34}$$

Explicit expressions for all N^B_{n-1} and q_{n-1}, for $n = 2, 4, 6$, are given in Appendix B. The resulting expansion coefficients for the pressure are shown in Fig. 8. Also shown in the bottom-right panel of this figure is the ratio of the expansion coefficients for the net baryon-number density, N^B_{n-1}, and the

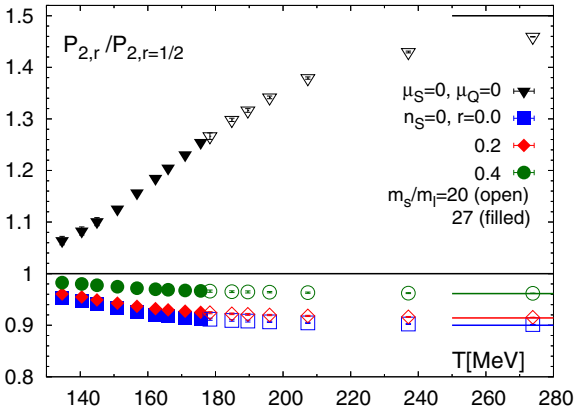

FIG. 9. Ratio of $\mathcal{O}(\hat{\mu}_B^2)$ expansion coefficients of the pressure in systems with electric charge to net baryon-number ratio $r = n_Q/n_B$ relative to that of strangeness neutral, isospin symmetric systems ($r = 1/2$). Triangles show the ratio of the pressure in systems with vanishing electric charge and strangeness chemical potential and the strangeness neutral, isospin symmetric system. Horizontal lines at high temperature show the corresponding free quark gas values. All data points shown are from calculations on lattices with temporal extent $N_\tau = 8$.

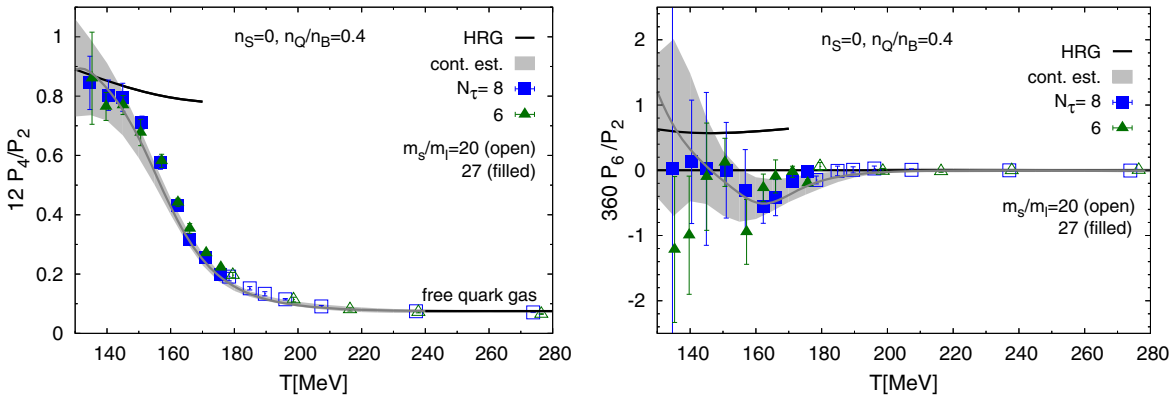

FIG. 10. Ratio of expansion coefficients of the pressure in strangeness neutral systems with $r = 0.4$. The darker lines in the center of the error bands of these extrapolations show results obtained with the parametrization discussed in Sec. V B.

appropriately rescaled expansion coefficients of the pressure, nP_n. In electric charge neutral systems, $r = 0$ as well as in the isospin symmetric limit $r = 1/2$, for which the expansion coefficients $q_i = 0$ vanish for all i, this ratio is unity. In both cases the simple relation given in Eq. (25) holds. Also for other values of r, the contribution from terms proportional to r are small. In Fig. 8 (bottom right) we show the ratio N^B_{2n-1}/nP_n for the case $r = 0.4$ and $n = 2$ and 4, respectively. At $\mathcal{O}(\hat{\mu}_B^2)$, differences between N^B_1 and $2P_2$ never exceed 2%, and at $\mathcal{O}(\hat{\mu}_B^4)$, the difference between N^B_3 and $4P_4$ varies between 3% at low temperature and −6% at high temperature. In the infinite temperature ideal gas limit the ratios become $N^B_1/2P_2 = 1.018$ and $N^B_3/4P_4 = 0.927$, respectively.

In general one finds that the dependence of bulk thermodynamic observables on the net electric charge to net baryon number-ratio is weak. The $\mathcal{O}(\hat{\mu}_B^2)$ expansion coefficient of the pressure in strangeness neutral systems differs by at most 10% in electric charge neutral ($r = 0$) and isospin symmetric systems ($r = 1/2$), respectively. The expansion coefficient P_2 evaluated for different values of r is shown in Fig. 9. For chemical potentials $\hat{\mu} \leq 2$, this amounts to differences less than 1.5% of the total pressure. On the other hand, strangeness neutral systems differ substantially from systems with vanishing strangeness chemical potential. In this case the $\mathcal{O}(\hat{\mu}_B^2)$ expansion coefficients differ by almost 50% in the high temperature limit. For $T < 150$ MeV, this difference is only about 10% reflecting that the different treatment of the strangeness sector becomes less important for the thermodynamics at low temperature. This is also shown in Fig. 9.

Compared to the leading $\mathcal{O}(\hat{\mu}_B^2)$ contributions to bulk thermodynamic observables, the $\mathcal{O}(\hat{\mu}_B^4)$ and $\mathcal{O}(\hat{\mu}_B^6)$ corrections are smaller in the strangeness neutral case than in the case $\mu_Q = \mu_S = 0$, which we have discussed in the previous section. This is evident from Fig. 10, where we show the ratios $12P_4/P_2$ and $360P_6/P_2$. These combinations are unity in a HRG with $\mu_S = \mu_Q = 0$ but smaller than unity in the strangeness neutral case. Higher-order corrections in Taylor series for strangeness neutral systems thus are of less importance than in the case $\mu_S = 0$. This also means that the errors, which are large on e.g. sixth-order expansion coefficients, are of less importance for the overall error budget of Taylor expansions in strangeness neutral systems. This is indeed reflected in the μ_B-dependence of $(P(T,\mu_B) - P(T,0))/T^4$ and $n_B(T,\mu_B)/T^3$ shown in the upper panels of Fig. 11 for the case $r = 0.4$. As can be seen in these two figures, at low temperatures the μ_B-dependent part of the pressure as well as the net baryon-number density agree quite well with HRG model calculations that describe the thermodynamics of a gas of noninteracting, pointlike hadron resonances. This agreement, however, gets worse at larger values of μ_B. Not unexpectedly, at higher temperatures deviations from HRG model calculations become large already at small values of μ_B. This is apparent from the lower two panels of Fig. 11, where we show the ratio of the μ_B-dependent part of the pressure and the corresponding HRG model result (left) and the net baryon-number density divided by the corresponding HRG model result (right). In the HRG model calculation $(P(T,\mu_B) - P(T,0))/T^4$ as well as $n_B(T,\mu_B)/T^3$ only depend on the baryon sector of the hadron spectrum. The results shown in Fig. 11 thus strongly suggest that HRG model calculations using resonance spectra in model calculations for noninteracting, pointlike hadron gases may be appropriate (within ∼10% accuracy) to describe the physics in the crossover region of strongly interacting matter at vanishing or small values of the baryon chemical potential, but fail[3]

[3]It has been pointed out that the pointlike particle approximation is appropriate in the meson sector but not in the baryon sector at high density. Introducing a nonzero size of hadron resonances [28,29] may, for some observables, improve the comparison with QCD thermodynamics [30,31]. However, it seems that the introduction of several additional parameters will be needed to achieve overall good agreement with the many observables calculated now in QCD in the temperature range of interest, i.e. in the crossover region from a hadron gas to strongly interacting quark-gluon matter.

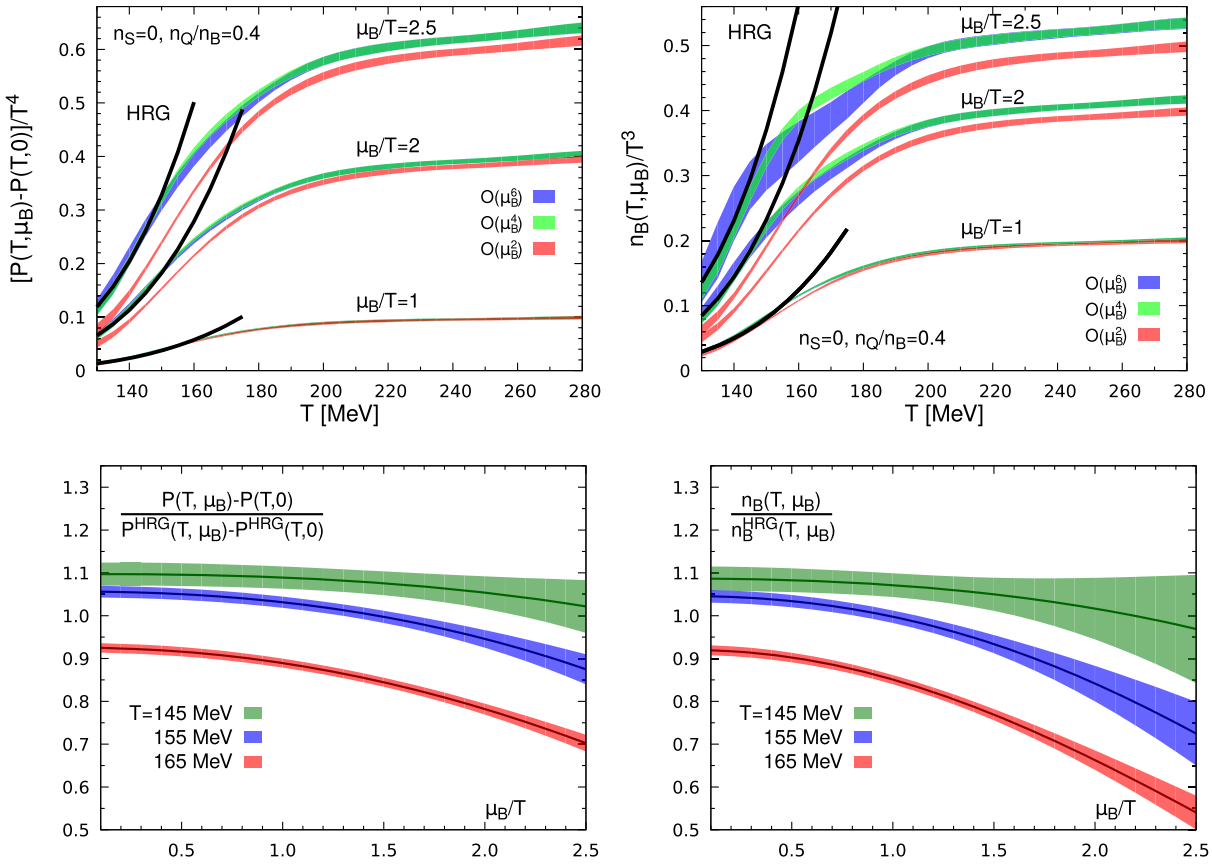

FIG. 11. The μ_B-dependent contribution to the pressure (top left) and the baryon-number density (top right) for several values of the baryon chemical potential in units of temperature. The lower two panels show these quantities normalized to the corresponding HRG model values, obtained from a calculation with all baryon resonances, up to mass $m_H = 2.5$ GeV, listed in the PDG tables, as function of μ_B/T for three values of the temperature.

to do so at large μ_B/T and/or $T \gtrsim 160$ MeV. At $T = 165$ MeV, QCD and HRG model results for the net baryon-number density differ by 40% at $\mu_B/T = 2$. This has consequences for the determination of freeze-out conditions in heavy ion collisions. We come back to this discussion in Sec. VI.

The μ_B-dependent contributions to the energy and entropy densities have been defined in Eqs. (23) and (24). In strangeness neutral systems the expansion coefficients simplify considerably,

$$\epsilon_{2n}(T) = 3P_{2n}(T) + TP'_{2n}(T) - r\sum_{k=1}^{n} Tq'_{2k-1}N^B_{2n-2k+1} \quad (35)$$

$$\sigma_{2n}(T) = 4P_{2n}(T) + TP'_{2n}(T) - N^B_{2n-1} - r\sum_{k=1}^{n}(q_{2k-1} + Tq'_{2k-1})N^B_{2n-2k+1}. \quad (36)$$

Results for the $\mathcal{O}(\mu_B^2)$ and $\mathcal{O}(\mu_B^4)$ expansion coefficients are shown in Fig. 12 together with the corresponding expansion coefficients for the pressure and net baryon-number density. Results for the total energy density as well as the total pressure for $\mu_B/T = 0$ and 2 are shown in Fig. 13. As discussed in the previous section also, here it is evident that current errors on the total pressure and energy density are dominated by errors on these observables at $\mu_B = 0$.

In Fig. 13 we also show results for the total pressure obtained within the stout discretization scheme. The result for $\hat{\mu}_B = 0$ is taken from [2]. The $\hat{\mu}_B$-dependent contribution is based on calculations with an imaginary chemical potential [14]. These results have been analytically continued to real values of $\hat{\mu}_B$ using a sixth-order polynomial in $\hat{\mu}_B$. As can be seen, the total pressure agrees quite well with the results obtained with a sixth-order Taylor expansion, although the results obtained the analytic continuation within the stout discretization scheme tend to stay systematically below the central values obtained from the analysis of Taylor series expansions in the HISQ discretization scheme.

B. Parametrization of the equation of state

At $\mu_B = 0$, the HotQCD Collaboration presented a parametrization of the pressure, obtained as interpolating

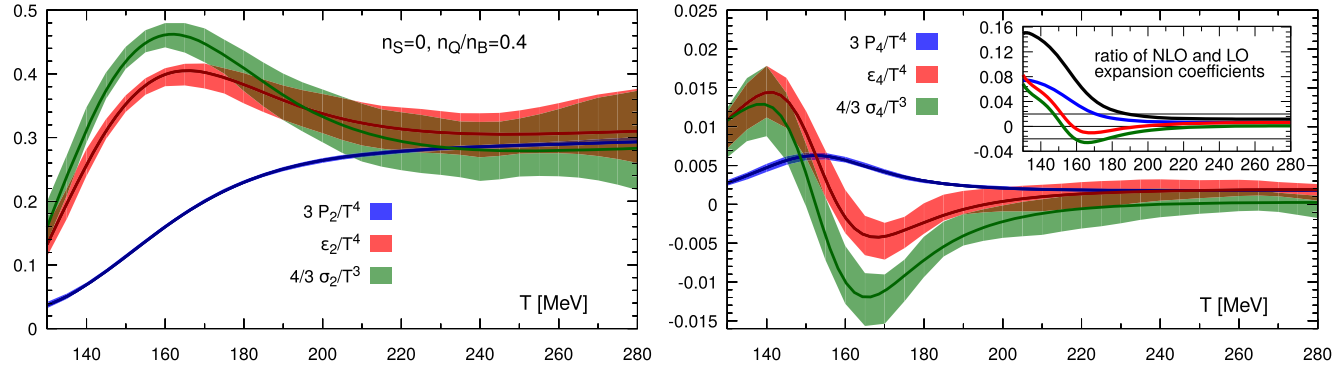

FIG. 12. Leading order (left) and next-to-leading order (right) expansion coefficients for the μ_B-dependent part of pressure, the energy and entropy densities in the strangeness neutral case with fixed electric charge to net baryon-number density, $n_Q/n_B = 0.4$. The darker lines in the center of the error bands of these extrapolations show the interpolating fits discussed in Sec. V B. The insert in the right-hand figure shows the ratios of NLO and LO expansion coefficients N_3^B/N_1^B, P_4/P_2, ϵ_4/ϵ_2 and σ_4/σ_2. The influence of a nonvanishing electric charge chemical potential, which formally gives rise to deviations from the result in the isospin symmetric limit ($N_1^B = 2P_2$, $N_3^B = 4P_4$), are negligible at $\mathcal{O}(\hat{\mu}_B^2)$ and $\mathcal{O}(\hat{\mu}_B^4)$. For that reason, we do not show results for N_1^B and N_3^B. However, we show in the insertion in the left-hand figure the ratio N_3^B/N_1^B (black line) which clearly shows that NLO corrections are a factor two larger in the Taylor series for the number density then in the pressure series.

curves for the continuum extrapolated fit, that also provided an adequate description of all the other basic thermodynamic quantities, i.e. the energy and entropy densities as well as the specific heat and the velocity of sound [3]. Here, we want to extend this parametrization to the case $\hat{\mu}_B > 0$. Similar to what has been done at $\mu_B = 0$, it turns out that a ratio of fourth-order polynomials in the inverse temperature is flexible enough to describe the temperature dependence of all required Taylor expansion coefficients in the temperature range $T \in [130\ \text{MeV}, 280\ \text{MeV}]$. We use such an ansatz for the three expansion coefficients of the net baryon-number density (N_1^B, N_3^B, N_5^B) and the three electric charge chemical potentials $(q_1,\ q_3,\ q_5)$. This suffices to calculate all thermodynamic observables in strangeness neutral systems.

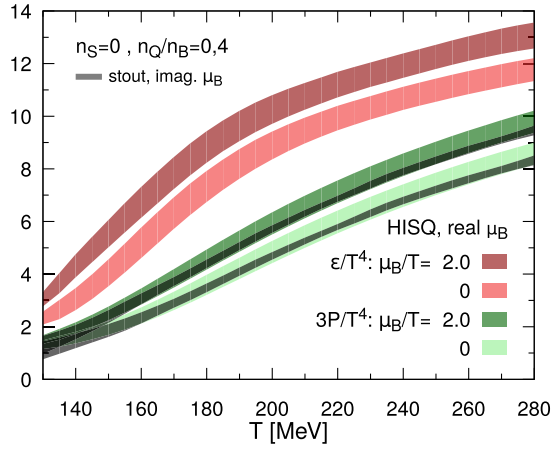

FIG. 13. The total energy density (upper two curves) of $(2+1)$-flavor QCD for $\mu_B/T = 0$ and 2, respectively. The lower two curves show corresponding results for three times the pressure. The dark lines show the results obtained with the stout action from analytic continuation with sixth-order polynomials in $\hat{\mu}_B$ [14].

We use a ratio of fourth-order polynomials in $1/T$ as an ansatz for the expansion coefficients of the net baryon-number density,

$$N_k^B(T) = \frac{N_{k,0n}^B + N_{k,1n}^B \bar{t} + N_{k,2n}^B \bar{t}^2 + N_{k,3n}^B \bar{t}^3 + N_{k,4n}^B \bar{t}^4}{1 + N_{k,1d}^B \bar{t} + N_{k,2d}^B \bar{t}^2 + N_{k,3d}^B \bar{t}^3 + N_{k,4d}^B \bar{t}^4}, \quad k = 1, 3, 5. \tag{37}$$

Here, $\bar{t} = T_c/T$, and the QCD transition temperature $T_c = 154$ MeV is used as a convenient normalization. Similarly, we define the parametrization of the expansion coefficients for the electric charge chemical potential,

$$q_k(T) = \frac{q_{k,0n} + q_{k,1n} \bar{t} + q_{k,2n} \bar{t}^2 + q_{k,3n} \bar{t}^3 + q_{k,4n} \bar{t}^4}{1 + q_{k,1d} \bar{t} + q_{k,2d} \bar{t}^2 + q_{k,3d} \bar{t}^3 + q_{k,4d} \bar{t}^4}, \quad k = 1, 3, 5. \tag{38}$$

The parameters for these interpolating curves are summarized in Table I.

The expansion coefficients of the pressure are then obtained by using Eqs. (32)–(34). The resulting interpolating curves for P_k are shown as darker curves in Fig. 8. All other interpolating curves shown as darker curves in other figures have been obtained by using the above interpolations. In particular, interpolating curves for the energy and entropy densities are obtained by using Eqs. (35) and (36) and calculating analytically temperature derivatives of the parametrizations of P_n and q_n given in Eqs. (37) and (38). The resulting interpolating curves for the second- and

TABLE I. Parameters used in the ansatz given in Eq. (37) for the interpolation of the expansion coefficients of the net baryon-number density of $(2+1)$-flavor QCD with vanishing net strangeness and a fixed ratio of electric charge and net baryon-number density, $n_Q/n_B = 0.4$. These interpolations have been determined for the temperature interval $T \in [130\ \text{MeV}, 280\ \text{MeV}]$. Also given are parameters needed for the interpolation of the expansion coefficients for the electric charge chemical potential [Eq. (38)] and the coefficients for the parametrization of the pressure at $\mu_B = 0$ given in Eq. (39).

k	$N^B_{k,0n}$	$N^B_{k,1n}$	$N^B_{k,2n}$	$N^B_{k,3n}$	$N^B_{k,4n}$	$N^B_{k,1d}$	$N^B_{k,2d}$	$N^B_{k,3d}$	$N^B_{k,4d}$
1	0.302182	−0.929305	1.230560	−0.798724	0.204722	−2.011836	1.190147	0.003869	−0.076244
3	0.000446650	0.00983742	−0.0315076	0.0323632	−0.0107642	−1.327047	0.0472047	0.0	0.323696
5	0.0000104211	−0.000327321	0.00122751	−0.00158725	0.000672708	−1.467875	−0.264770	0.796010	−0.044968
k	$q_{k,0n}$	$q_{k,1n}$	$q_{k,2n}$	$q_{k,3n}$	$q_{k,4n}$	$q_{k,1d}$	$q_{k,2d}$	$q_{k,3d}$	$q_{k,4d}$
1	−0.114472	−0.631833	2.102001	−2.165174	0.739905	16.565265	−35.328733	19.940335	0.384797
3	0.0505332	−0.312052	0.700958	−0.662171	0.219351	−23.224117	82.688725	−89.160400	31.381036
5	0.0000842	−0.0005250	0.00113467	−0.00103897	0.00034414	−2.095094	0.987940	0.146830	−0.0210650
	p_{0n}	p_{1n}	p_{2n}	p_{3n}	p_{4n}	p_{1d}	p_{2d}	p_{3d}	p_{4d}
0	0.00556035	128.702341	−293.064074	228.763685	−58.084225	12.713331	0.0	−31.330957	26.524394

fourth-order Taylor expansion coefficients are shown in Fig. 12.

We also used a ratio of fourth-order polynomials to interpolate results for the pressure at $\mu_B = 0$. We write the pressure as

$$\frac{P(T,\mu_B=0)}{T^4} = \frac{p_{0n} + p_{1n}\bar{t} + p_{2n}\bar{t}^2 + p_{3n}\bar{t}^3 + p_{4n}\bar{t}^4}{1 + p_{1d}\bar{t} + p_{2d}\bar{t}^2 + p_{3d}\bar{t}^3 + p_{4d}\bar{t}^4}. \quad (39)$$

The coefficients p_{in} and p_{id} are also given in Table I.

VI. LINES OF CONSTANT PHYSICS TO $\mathcal{O}(\mu_B^4)$

We use here the Taylor series for bulk thermodynamic observables, i.e. the pressure, energy and entropy densities, to discuss contour lines in the T-μ_B plane on which these observables stay constant. It has been argued quite successfully that the thermal conditions at the time of chemical freeze-out in heavy ion collisions can be characterized by lines in the T-μ_B plane on which certain thermodynamic observables or ratios thereof stay constant [32,33], although the freeze-out mechanism in the rapidly expanding fireball created in a heavy ion collision is of dynamical origin and will in detail be more complicated (see, for instance, [34]). While lines of constant physics (LCPs) involving total baryon-number densities, as used in [32,33], are not appropriate for calculations within the framework of quantum field theories, other criteria like lines of constant entropy density in units of T^3 [35] or constant pressure [36–38] have been suggested to characterize freeze-out parameters (T_f, μ_B^f) corresponding to heavy ion collisions at different values of the beam energy ($\sqrt{s_{NN}}$). Generally, such criteria have been established by comparing experimental data with model calculations based on some version of a HRG model. We determine here LCPs from the lattice QCD calculations of pressure, energy and entropy densities and confront them with freeze-out parameters that have been obtained by comparing particle yields, measured at different values of $\sqrt{s_{NN}}$, to HRG model calculations.

We consider an observable $f(T,\mu_B)$, i.e. the pressure, energy density or entropy density which are even functions of μ_B. We parametrize a "line of constant f" by

$$T_f(\mu_B) = T_0\left(1 - \kappa_2^f\left(\frac{\mu_B}{T_0}\right)^2 - \kappa_4^f\left(\frac{\mu_B}{T_0}\right)^4\right). \quad (40)$$

In order to determine the expansion coefficients κ_2^f and κ_4^f we need to expand the function $f(T,\mu_B)$ up to fourth-order in μ_B and up to second-order in T around some point $(T_0, 0)$,

$$\begin{aligned} f(T,\mu_B) = {} & f(T_0,0) + \left.\frac{\partial f(T,\mu_B)}{\partial T}\right|_{(T_0,0)}(T-T_0) + \frac{1}{2}\left.\frac{\partial^2 f(T,\mu_B)}{\partial \mu_B^2}\right|_{(T_0,0)}\mu_B^2 \\ & + \frac{1}{2}\left.\frac{\partial^2 f(T,\mu_B)}{\partial T^2}\right|_{(T_0,0)}(T-T_0)^2 + \frac{1}{2}\frac{\partial}{\partial T}\left.\frac{\partial^2 f(T,\mu_B)}{\partial \mu_B^2}\right|_{(T_0,0)}(T-T_0)\mu_B^2 + \frac{1}{4!}\left.\frac{\partial^4 f(T,\mu_B)}{\partial \mu_B^4}\right|_{(T_0,0)}\mu_B^4. \end{aligned} \quad (41)$$

Note that we expand here in terms of μ_B rather than in $\hat{\mu}_B \equiv \mu_B/T$. Replacing the temperature T in Eq. (41) by the ansatz for a line of constant f, Eq. (40), and keeping terms up to $\mathcal{O}(\mu_B^4)$ gives

$$f(T(\mu_B),\mu_B) = f(T_0,0) + \left(-\kappa_2^f \frac{\partial f(T,\mu_B)}{\partial T}\bigg|_{(T_0,0)} \frac{1}{T_0} + \frac{1}{2}\frac{\partial^2 f(T,\mu_B)}{\partial \mu_B^2}\bigg|_{(T_0,0)} \right)\mu_B^2$$
$$+ \left(-\kappa_4^f \frac{\partial f(T,\mu_B)}{\partial T}\bigg|_{(T_0,0)} \frac{1}{T_0^3} + \frac{1}{2}\frac{\partial^2 f(T,\mu_B)}{\partial T^2}\bigg|_{(T_0,0)} (\kappa_2^f)^2 \frac{1}{T_0^2} - \frac{1}{2}\frac{\partial}{\partial T}\frac{\partial^2 f(T,\mu_B)}{\partial \mu_B^2}\bigg|_{(T_0,0)} \kappa_2^f \frac{1}{T_0} + \frac{1}{4!}\frac{\partial^4 f(T,\mu_B)}{\partial \mu_B^4}\bigg|_{(T_0,0)} \right)\mu_B^4.$$

We then can determine κ_2^f and κ_4^f by demanding that the expansion coefficients at $\mathcal{O}(\mu_B^2)$ and $\mathcal{O}(\mu_B^4)$ vanish; i.e.

$$\kappa_2^f = \frac{T_0}{2}\frac{\frac{\partial^2 f(T,\mu_B)}{\partial \mu_B^2}|_{(T_0,0)}}{\frac{\partial f(T,\mu_B)}{\partial T}|_{(T_0,0)}}, \tag{42}$$

$$\kappa_4^f = \frac{\frac{1}{2}T_0^2\frac{\partial^2 f(T,\mu_B)}{\partial T^2}|_{(T_0,0)}(\kappa_2^f)^2 - \frac{1}{2}T_0^3\frac{\partial}{\partial T}\frac{\partial^2 f(T,\mu_B)}{\partial \mu_B^2}|_{(T_0,0)}\kappa_2^f + \frac{1}{4!}T_0^4\frac{\partial^4 f(T,\mu_B)}{\partial \mu_B^4}|_{(T_0,0)}}{T_0\frac{\partial f(T,\mu_B)}{\partial T}|_{(T_0,0)}}. \tag{43}$$

As we deal with observables that are given as a Taylor series in $\hat{\mu}_B$ at fixed T, i.e. $f(T,\mu_B) = \sum_{k=0}^{\infty} f_{2k}(T)\hat{\mu}_B^{2k}$, the derivatives with respect to μ_B appearing in Eqs. (42) and (43) can be replaced by suitable Taylor expansion coefficients of $f(T,\mu_B)$,

$$\kappa_2^f = \frac{f_2(T_0)}{T_0\frac{\partial f_0(T)}{\partial T}|_{(T_0,0)}} \tag{44}$$

$$\kappa_4^f = \frac{\frac{1}{2}T_0^2\frac{\partial^2 f_0(T)}{\partial T^2}|_{(T_0,0)}(\kappa_2^f)^2 - (T_0\frac{\partial f_2(T)}{\partial T}|_{(T_0,0)} - 2f_2(T_0))\kappa_2^f + f_4(T_0)}{T_0\frac{\partial f_0(T)}{\partial T}|_{(T_0,0)}}. \tag{45}$$

We in the following work out detailed expressions for the quadratic correction coefficient, κ_2^f, for lines of constant pressure ($f \equiv P$), energy density ($f \equiv \epsilon$) and entropy density ($f \equiv s$) in strangeness neutral systems with electric charge to net baryon-number ratio $r = 0.4$. Details for the quartic coefficient, κ_4^f, are given in Appendix C.

Pressure $f \equiv P$: The function $f(T,\mu_B)$ is given by $P = T^4\sum_n P_n(\mu_B/T)^n$, with $P_0 = P(T,0)/T^4$ denoting the pressure in units of T^4 at vanishing baryon chemical potential and $P_n(T)$, $n > 0$ denoting the expansion coefficients of $P(T,\mu_B)/T^4$ as introduced in Eq. (15). In the denominator of Eq. (44) we use the thermodynamic relation between pressure and entropy density $s = (\partial P/\partial T)_{\mu_B}$. The numerator is given by $f_2(T) = T^4 P_2(T)$. This gives

$$\kappa_2^P = \frac{P_2}{s/T^3}, \tag{46}$$

where s/T^3 is evaluated at $\hat{\mu}_B = 0$.

Energy density $f \equiv \epsilon$: The function $f(T,\mu_B)$ is given by $\epsilon = T^4\sum_n \epsilon_n(\mu_B/T)^n$, with $\epsilon_0 = \epsilon(T,0)/T^4$ denoting the energy density in units of T^4 at vanishing baryon chemical potential. In the denominator of Eq. (44) we use the thermodynamic relation between energy density and specific heat $C_V = (\partial\epsilon/\partial T)_{\mu_B}$ In the numerator we have $f_2(T) = T^4\epsilon_2(T)$. This gives

$$\kappa_2^\epsilon = \frac{\epsilon_2}{C_V/T^3}, \tag{47}$$

where C_V/T^3 is evaluated at $\hat{\mu}_B = 0$.

Entropy density $f \equiv s$: The function $f(T,\mu_B)$ is given by $s = (\epsilon + P - \mu_B n_B - \mu_Q n_Q)/T = (\epsilon + P - \mu_B n_B(1 + r\mu_Q/\mu_B))/T$. As n_B is of $\mathcal{O}(\mu_B)$, we need for the ratio of electric charge and strangeness chemical potentials only the leading order relation $\mu_Q/\mu_B = q_1$ defined in Eq. (14). In the denominator we use

$$\frac{\partial s}{\partial T} = \frac{\partial(\epsilon+P)/T}{\partial T} = -\frac{s}{T} + \frac{1}{T}\frac{\partial(\epsilon+P)}{\partial T} = \frac{C_V}{T}. \tag{48}$$

In the numerator we have $f_2(T) = T^3(\epsilon_2 + P_2 - N_1^B(1 + rq_1))$. With this we get

$$\kappa_2^s = T^3\frac{\epsilon_2 + P_2 - N_1^B(1+rq_1)}{C_V} = \frac{\epsilon_2 - P_2}{C_V/T^3}, \tag{49}$$

where we have used Eq. (32) to replace N_1^B in favor of P_2.

We note that $\kappa_2^\epsilon > \kappa_2^s$, i.e. with increasing μ_B, the entropy density decreases on lines of constant energy density.

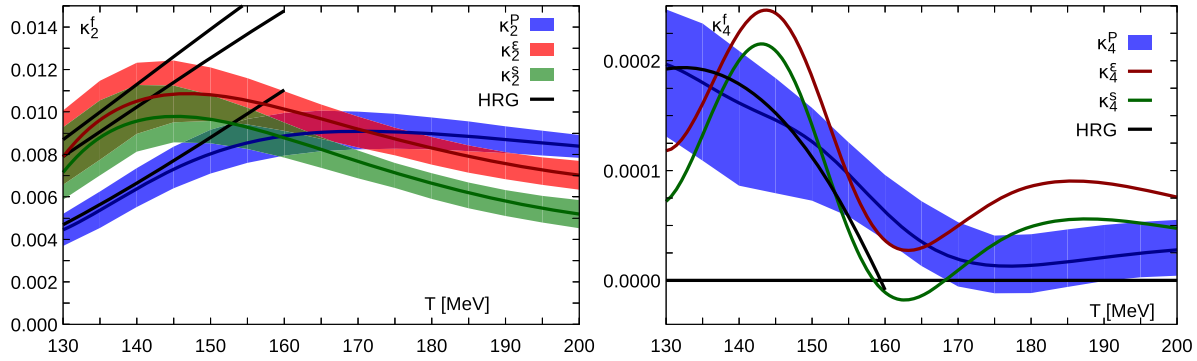

FIG. 14. (Left) Second-order curvature coefficients of lines of constant pressure, energy density and entropy density versus temperature in $(2+1)$-flavor QCD (bands) and in a HRG model (lines). (Right) Same as on the left, but for fourth-order coefficients. The darker lines in the center of the error bands show the interpolating fits discussed in Sec. V B. For κ_4^ϵ and κ_4^s, only these interpolating curves are shown.

The second-order coefficients for the lines of constant physics thus can directly be calculated using the continuum extrapolated results for the pressure and energy density obtained at vanishing chemical potential in [3] and the leading order expansion coefficient of the pressure shown in Fig. 10. Similarly, we obtain the quartic coefficients from the fourth-order expansion of the pressure using the relations given in Appendix C. We show results for κ_2^f and κ_4^f in Fig. 14.

In the interval around T_c, i.e. $T \in [145\ \text{MeV}, 165\ \text{MeV}]$, we find

$$\begin{aligned} 0.0064 &\le \kappa_2^P \le 0.0101, \\ 0.0087 &\le \kappa_2^\epsilon \le 0.012, \\ 0.0074 &\le \kappa_2^s \le 0.011. \end{aligned} \tag{50}$$

Apparently, at $\mathcal{O}(\mu_B^2)$, lines of constant pressure and constant energy or entropy densities agree quite well, and they also agree, within currently large errors, with the curvature of the transition line in $(2+1)$-flavor QCD. The coefficient of the quartic correction for the contour lines turns out to be about two orders of magnitude smaller than the leading order coefficients. This, of course, reflects the small contribution of the NLO corrections to the μ_B-dependent part of pressure and energy density. For all fourth-order coefficients, we find $|\kappa_4^f| \le 0.00024$ in the temperature interval around T_c. For $\mu_B/T \le 2$, the contribution arising from κ_4^f only leads to modifications of $T_f(\mu_B)$ that stays within the error band arising from the uncertainty in κ_2^f.

The resulting lines of constant physics in the T-μ_B plane are shown in Fig. 15 (left) for three values of the

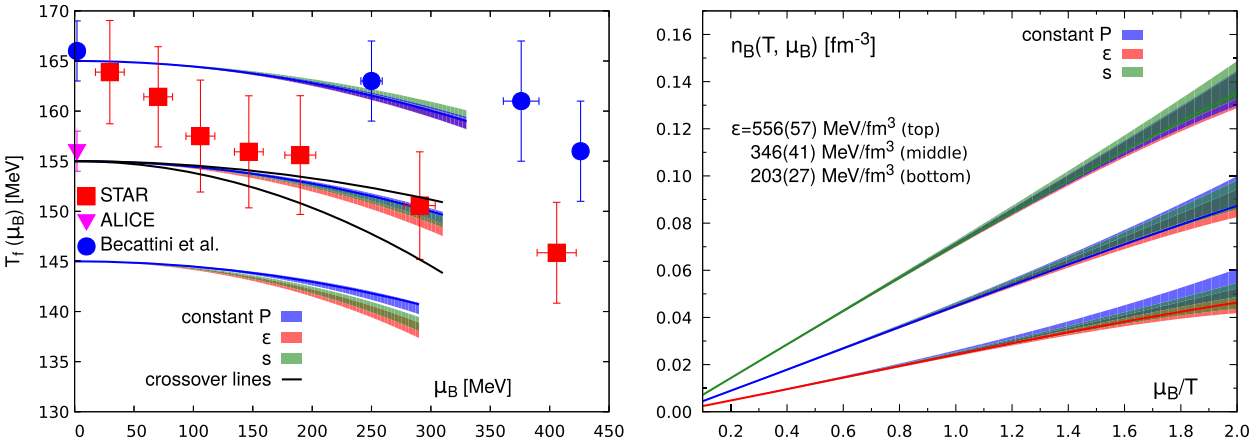

FIG. 15. (Left) Lines of constant pressure, energy density and entropy density versus temperature in $(2+1)$-flavor QCD for three different initial sets of values fixed at $\mu_B = 0$ and $T_0 = 145$, 155 and 165 MeV, respectively (see Table II). Data points show freeze-out temperatures determined by the STAR Collaboration in the BES at RHIC (squares) [39] and the ALICE Collaboration at the LHC (triangles) [40]. The circles denote hadronization temperatures obtained by comparing experimental data on particle yields with a hadronization model calculation [41]. Also shown are two lines representing the current spread in determinations of the μ_B-dependence of the QCD crossover transition line (see text). (Right) Net baryon-number density on the lines of constant physics for three values of the energy density at $\mu_B = 0$. Other thermodynamic parameters characterizing these lines are summarized in Table II.

temperature, $T = 145$, 155 and 165 MeV. These correspond to constant energy densities $\epsilon = 0.203(27)$, 0.346 (41) and 0.556(57) GeV/fm^3, which roughly correspond to the energy density of cold nuclear matter, a hard sphere gas of nucleons at dense packing and the interior of a nucleus, respectively. Values of other bulk thermodynamic observables characterizing these LCPs are summarized in Table II. The corresponding net baryon-number densities on these LCPs are shown in Fig. 15 (right). It is apparent from Fig. 15 (left) that LCPs for constant pressure, energy or entropy density agree well with each other up to baryon chemical potentials $\mu_B/T = 2$, where the difference in temperature on different LCPs is at most 2 MeV. We also note that the temperature on a LCP varies by about 7 MeV or, equivalently, 5% between $\hat{\mu}_B = 0$ and $\hat{\mu}_B = 2$. Thus, on a line of constant pressure, the entropy in units of T^3 changes by about 15%. That is, constant P or constant s/T^3, which both have been suggested as phenomenological descriptions for freeze-out conditions in heavy ion collisions, cannot hold simultaneously, although a change of 15% of one of these observables may phenomenologically not be of much relevance. We also stress that at large values of $\hat{\mu}_B$ the comparison of experimental data with HRG model calculations, e.g. the use of single particle Boltzmann distributions used to extract freeze-out temperatures and chemical potentials, becomes questionable. As shown in Fig. 11, net baryon-number densities extracted from HRG and QCD calculations differ substantially at $\mu_B/T \simeq 2$.

Also shown in Fig. 15 (left) are results on freeze-out parameters and hadronization temperatures extracted from particle yields measured in heavy ion experiments [39–41] by comparing data with model calculations based on the hadron resonance gas models. The region $\mu_B/T \leq 2$ corresponds to beam energies $\sqrt{s_{NN}} \geq 11.4$ GeV in the RHIC beam energy scan. Obviously, the freeze-out parameters extracted from the beam energy scan data [39] do not follow any of the LCPs. However, the discrepancy between the freeze-out parameters determined at the LHC [40] and the highest beam energy at RHIC [39] suggests that also these determinations are not consistent among each other.

Finally, we note that the lines of constant physics discussed above compare also well with the crossover line for the QCD transition. At nonzero values of the baryon chemical potential the change of the (pseudo)critical temperature has been determined, using various approaches at real [42,43] and imaginary [44–46] values of the chemical potential. To leading order one obtains

$$T_c(\mu_B) = T_c(0)\left(1 - \kappa_2^c\left(\frac{\mu_B}{T_c(0)}\right)^2\right), \qquad (51)$$

with κ_2^c ranging from 0.0066(7) [42,43] to 0.0135(20) [44], 0.0149(21) [45] and 0.020(4) [46]. Lines that cover this spread in curvature parameters are also shown in Fig. 15 (left) for $T_c(0) = 155$ MeV. While a small curvature for the crossover line would suggest that the crossover transition happens under more or less identical bulk thermodynamic conditions, a large curvature obviously would indicate that the crossover transition happens already at significantly smaller values of pressure and energy density as μ_B/T increases.

VII. RADIUS OF CONVERGENCE AND THE CRITICAL POINT

As discussed in the previous sections, we generally find that the Taylor series for all basic thermodynamic quantities converge well for values of baryon chemical potentials $\mu_B \leq 2T$. Even in the low temperature regime, the relative contribution of higher-order expansion coefficients are generally smaller than in corresponding HRG model calculations. This, of course, also has consequences for our current understanding of the location of a possible critical point in the QCD phase diagram.

The results on the expansion coefficients of the Taylor series for, e.g., the pressure can be cast into estimates for the location of a possible critical point in the QCD phase diagram. In general the radius of convergence can be obtained from ratios of subsequent expansion coefficients in the Taylor series for the pressure. Equally well, one may use one of the derivatives of the pressure series. As one has to rely on estimates of the radius of convergence that generally are based on a rather short series, it may indeed be advantageous to use as a starting point the series for the net baryon-number susceptibility [47], which diverges at the critical point, but still contains information from all expansion coefficients of the pressure series. The radius of convergence of this series is identical to that of the pressure. Model calculations also suggest that the estimators obtained

TABLE II. Pressure, energy density and entropy density, characterizing lines of constant physics which correspond to the conditions met for $\mu_B = 0$ at $T_0 = 145$, 155 and 165 MeV. Columns 2–4 give results in appropriate units of temperature, while columns 5–7 give the same results expressed in units of GeV and fm.

	at $\mu_B = 0$			on LCP		
T_0[MeV]	p/T_0^4	ϵ/T_0^4	s/T_0^3	p[GeV/fm^3]	ϵ[GeV/fm^3]	s[fm^{-3}]
145	0.586(80)	3.52(47)	4.11(53)	0.0337(46)	0.203(27)	1.63(21)
155	0.726(95)	4.61(55)	5.34(63)	0.0546(71)	0.346(41)	2.59(30)
165	0.898(110)	5.76(59)	6.66(69)	0.0868(106)	0.556(57)	3.90(40)

from the susceptibility series converge faster to the true radius of convergence [48]. For $\mu_Q = \mu_S = 0$, the expansion coefficients of the Taylor series for the net baryon-number susceptibility are again simply related to that of the pressure,

$$\chi_2^B(T,\mu_B) = \sum_{n=0}^{\infty} \frac{1}{(2n)!} \chi_{2n+2}^B \hat{\mu}_B^{2n}. \tag{52}$$

From this, one obtains estimators for the radius of convergence of the pressure and susceptibility series,

$$r_{2n}^P = \left| \frac{(2n+2)(2n+1)\chi_{2n}^B}{\chi_{2n+2}^B} \right|^{1/2},$$
$$r_{2n}^\chi = \left| \frac{2n(2n-1)\chi_{2n}^B}{\chi_{2n+2}^B} \right|^{1/2}. \tag{53}$$

Both estimators converge to the true radius of convergence in the limit $n \to \infty$. In order for this to correspond to a singularity at real values of $\hat{\mu}_B$, all expansion coefficients should asymptotically stay positive.

Obviously, the estimators r_{2n}^P and r_{2n}^χ are proportional to each other, $r_{2n}^P = \sqrt{(2n+2)(2n+1)/[2n(2n-1)]}\, r_{2n}^\chi$. The difference between these to estimators may be taken as a systematic error for any estimate of the radius of convergence obtained from a truncated Taylor series. In the hadron resonance gas limit one finds for estimators involving sixth-order cumulants, $r_4^P = 1.58 r_4^\chi$. In the following we restrict our discussion to an analysis of r_{2n}^χ, which at finite n leads to the smaller estimator for the radius of convergence. This seems to be appropriate in the present situation where we only can construct two independent estimators from ratios of three distinct susceptibilities. We thus may hope to identify regions in the QCD phase diagram at small values of $\hat{\mu}_B$ which are unlikely locations for a possible critical point.

An immediate consequence of the definitions given in Eq. (53) is that the ratios of generalized susceptibilities need to grow asymptotically like $|\chi_{n+2}^B/\chi_n^B| \sim n^2$ in order to arrive in the limit $n \to \infty$ at a finite value for the radius of convergence. At least for large values of n, one thus needs to find large deviations from the hadron resonance gas results $|\chi_{n+2}^B/\chi_n^B|^{HRG} = 1$. As is obvious from the results presented in the previous sections, in particular from Fig. 3, the analysis of up to sixth-order Taylor expansion coefficients does not provide any hints for such large deviations. The ratio χ_4^B/χ_2^B turns out to be less than unity in the entire temperature range explored so far, i.e. for $T \geq 135$ MeV or $T/T_c > 0.87(6)$. Below the crossover temperature, $T \sim 155$ MeV, the sixth-order expansion coefficients also are consistent with HRG model results. They still have large errors. However, using the upper value of the error for χ_6^B/χ_4^B provides a lower limit for the value of the estimator r_4^χ. For temperatures in the interval 135 MeV $\leq T \leq$ 155 MeV (or equivalently $0.87(5) \leq T/T_c \leq 1$), we currently obtain a lower limit on r_4^χ from the estimate $\chi_6^B/\chi_4^B \simeq \chi_6^B/\chi_2^B < 3$. This converts into the bound $r_4^\chi \geq 2$, which is consistent with our observation that the Taylor series of all thermodynamic observables discussed in the previous sections is well behaved up to $\mu_B = 2T$. A more detailed analysis, using the current errors on χ_6^B/χ_4^B at five temperature values below and in the crossover region of the transition at $\mu_B = 0$, is shown in Fig. 16. This shows that the bound arising from r_4^χ is actually more stringent at temperatures closer to T_c, where χ_6 starts to become small and eventually tends to become negative.

These findings are consistent with recent results for susceptibility ratios obtained from calculations with an imaginary chemical potential [15]. Also in that case, all susceptibility ratios are consistent with HRG model results. At present, one thus cannot rule out that the radius of convergence may actually be infinite. Results for r_4^χ obtained in Ref. [15] lead to even larger estimators for the radius of convergence than our current lower bound. This is also shown in Fig. 16.

The observations and conclusions discussed above are in contrast to estimates for the location of a critical point obtained from a calculation based on a reweighting technique [49] as well as from Taylor series expansion in 2-flavor QCD [50,51]. Both these calculations have been performed with unimproved staggered fermion discretization schemes and thus may suffer from large cutoff effects. Moreover, the latter calculation also suffers from large statistical errors on higher order susceptibilities. Results from Refs. [49] and [50] are also shown in Fig. 16.

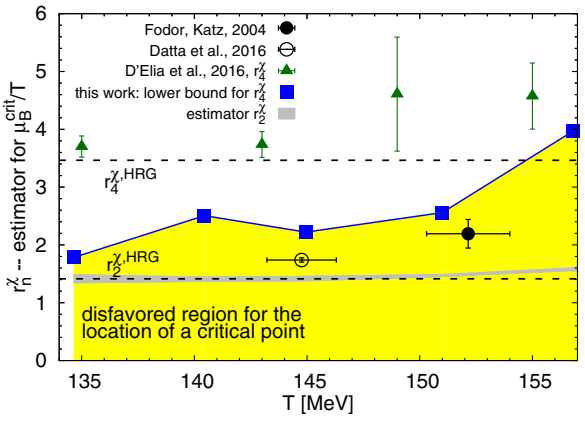

FIG. 16. Estimators for the radius of convergence of the Taylor series for net baryon-number fluctuations, $\chi_2^B(T,\mu_B)$, in the case of vanishing electric charge and strangeness chemical potentials obtained on lattices with temporal extent $N_\tau = 8$. Shown are lower bounds for the estimator r_4^χ obtained in this work (squares) and results for this estimator obtained from calculations with an imaginary chemical potential (triangles) [15]. Also shown are estimates for the location of the critical point obtained from calculations with unimproved staggered fermions using a reweighting technique [49] and Taylor expansions [50]. In both cases, results have been rescaled using $T_c = 154$ MeV.

We thus conclude from our current analysis that a critical point at chemical potentials smaller than $\mu_B = 2T$ is strongly disfavored in the temperature range 135 MeV $\leq T \leq$ 155 MeV, and its location at higher values of temperature seems to be ruled out. Our results suggest that the radius of convergence in that temperature interval will turn out to be significantly larger than the current bound once the statistics on sixth-order cumulants gets improved and higher-order cumulants become available.

VIII. CONCLUSIONS

We have presented results on the equation of state of strong-interaction matter obtained from a sixth-order Taylor expansion of the pressure of $(2+1)$-flavor QCD with physical light and strange quark masses. We discussed expansions at vanishing strangeness chemical potential $\mu_S = 0$ as well as for strangeness neutral systems $n_S = 0$. We have discussed in detail the latter case for a fixed electric charge to net baryon-number ratio, $n_Q/n_B = 0.4$, which is appropriate for situations met in heavy ion collisions. The results, however, can easily be extended to arbitrary ratios of n_Q/n_B. We find that the dependence of basic thermodynamic observables on n_Q/n_B is small for $0 \leq n_Q/n_B \leq 1/2$. This may be of interest for applications in heavy ion collisions where strong external magnetic fields and nontrivial topology in QCD can lead to charge asymmetries in different regions of phase space.

We have presented a parametrization of basic thermodynamic observables in terms of ratios of fourth-order polynomials in the inverse temperature which is appropriate in the temperature range studied here; i.e. $T \in [130$ MeV, 330 MeV$]$.

We presented results for lines of constant pressure, energy and entropy density in the T-μ_B plane and showed that corrections of $\mathcal{O}(\hat{\mu}_B^4)$ are negligible for $\hat{\mu}_B < 2$. For all three observables, the curvature term at $\mathcal{O}(\hat{\mu}_B^2)$ is smaller than $\kappa^{\max} = 0.012$. This suggest that, e.g., energy density and pressure would drop on the crossover line for the chiral transition, if the corresponding curvature coefficient turns out to be larger than $\kappa^{\max}$.

The Taylor series for pressure and net baryon-number density as well as energy density and entropy density determined for $\mu_S = 0$ as well as $n_S = 0$ have expansion coefficients that are close to HRG model results at low temperature. In general ratios of subsequent expansion coefficients approach the corresponding HRG model values from below when lowering the temperature. As a consequence, in the entire temperature range explored so far, the expansions are "better behaved" than the HRG model series, which have an infinite radius of convergence. Assuming that the current results obtained with expansion coefficients up to sixth-order are indicative for the behavior of higher-order expansion coefficients and taking into account the current errors on sixth-order expansion coefficients, we concluded that at temperatures $T > 135$ MeV the presence of a critical point in the QCD phase diagram for $\mu_B \leq 2T$ is unlikely.

ACKNOWLEDGMENTS

This work was supported in part through Contract No. DE-SC001270 with the U.S. Department of Energy, through the Scientific Discovery through Advanced Computing (SciDAC) program funded by the U.S. Department of Energy, Office of Science, Advanced Scientific Computing Research and Nuclear Physics, the DOE funded BEST Topical Collaboration, the NERSC Exascale Application Program (NESAP), the Grant No. 05P12PBCTA of the German Bundesministerium für Bildung und Forschung, the Grant No. 56268409 of the German Academic Exchange Service (DAAD), Grant No. 283286 of the European Union, the National Natural Science Foundation of China under Grants No. 11535012 and No. 11521064, and the Early Career Research Award of the Science and Engineering Research Board of the Government of India. Numerical calculations have been made possible through an INCITE grant of USQCD, ALCC grants in 2015 and 2016, and PRACE grants at CINECA, Italy, and the John von Neumann-Institute for Computing (NIC) in Germany. These grants provided access to resources on Titan at ORNL, BlueGene/Q at ALCF and NIC, Cori I and II at NERSC and Marconi at CINECA. Additional numerical calculations have been performed on USQCD GPU and KNL clusters at JLab and Fermilab, as well as GPU clusters at Bielefeld University, Paderborn University, and Indiana University. We furthermore acknowledge the support of NVIDIA through the CUDA Research Center at Bielefeld University.

APPENDIX A: DETAILS ON SIMULATION PARAMETERS AND DATA SETS

Our main data sets have been generated on lattices of size $N_\sigma^3 \times N_\tau$, with $N_\sigma/N_\tau = 4$ and $N_\tau = 6$, 8 and 12. We performed calculations with two different light to strange quark mass ratios, $m_l/m_s = 1/20$ and $1/27$, respectively. The simulation parameters are summarized in Tables III and IV.

TABLE III. Ensemble parameters for calculations with light to strange quark mass ratio $m_l/m_s = 1/20$ on lattices of size $N_\sigma^3 N_\tau$ with $N_\tau = 6$, 8 and $N_\sigma = 4N_\tau$. Columns 4 and 8 give the number of gauge field configurations, separated by 10 RHMC steps, that contributed to the analysis of up to sixth-order generalized susceptibilities χ_{ijk}^{BQS}.

$N_\tau = 6$				$N_\tau = 8$			
β	m_l	T[MeV]	#conf.	β	m_l	T[MeV]	#conf.
6.245	0.00415	179.52	14521	6.515	0.00302	178.36	16933
6.341	0.00370	198.61	3745	6.550	0.00291	184.84	15853
6.423	0.00335	216.33	1481	6.575	0.00282	189.58	11853
6.515	0.00302	237.81	1408	6.608	0.00271	196.01	16760
6.664	0.00257	276.43	1364	6.664	0.00257	207.32	8358
				6.800	0.00224	237.07	5816
				6.950	0.00193	273.88	9550
				7.150	0.00160	330.23	9184

TABLE IV. Same as Table III but for the light to strange quark mass ratio $m_l/m_s = 1/27$ and including results for $N_\tau = 12$.

$N_\tau = 6$				$N_\tau = 8$				$N_\tau = 12$			
β	m_l	T[MeV]	#conf.	β	m_l	T[MeV]	#conf.	β	m_l	T[MeV]	#conf.
5.980	0.00435	135.29	81200	6.245	0.00307	134.64	180320	6.640	0.00196	134.94	5834
6.010	0.00416	139.71	120790	6.285	0.00293	140.45	172110	6.680	0.00187	140.44	5833
6.045	0.00397	145.05	120770	6.315	0.00281	144.95	138150	6.712	0.00181	144.97	13846
6.080	0.00387	150.59	79390	6.354	0.00270	151.00	107510	6.754	0.00173	151.10	14200
6.120	0.00359	157.17	66180	6.390	0.00257	156.78	135730	6.794	0.00167	157.13	15476
6.150	0.00345	162.28	79660	6.423	0.00248	162.25	115850	6.825	0.00161	161.94	16772
6.170	0.00336	165.98	49760	6.445	0.00241	165.98	120270	6.850	0.00157	165.91	19542
6.200	0.00324	171.15	122700	6.474	0.00234	171.02	139980	6.880	0.00153	170.77	21220
6.225	0.00314	175.76	122730	6.500	0.00228	175.64	133070	6.910	0.00148	175.76	12303

APPENDIX B: CONSTRAINTS ON CHEMICAL POTENTIAL FOR STRANGENESS NEUTRAL SYSTEMS WITH FIXED ELECTRIC CHARGE TO BARYON-NUMBER RATIO

We are interested in expansion coefficients for strangeness neutral systems in which the net electric charge is proportional to the net baryon-number. That is, we introduce the constraint given in Eq. (31). These constraints can be fulfilled order by order in the Taylor expansion of the number densities by choosing the expansion coefficients of the series for $\hat{\mu}_Q$ and $\hat{\mu}_S$, given in Eq. (14), appropriately; i.e. the coefficients s_n and q_n can be determined order by order. We start with the Taylor series for the number densities introduced in Eq. (16) and define the expansion coefficients as

$$N_n^B = s_n\chi_{11}^{BS} + q_n\chi_{11}^{BQ} + m_n^B \tag{B1}$$

$$N_n^Q = s_n\chi_{11}^{QS} + q_n\chi_2^Q + m_n^Q \tag{B2}$$

$$N_n^S = s_n\chi_2^S + q_n\chi_{11}^{QS} + m_n^S \tag{B3}$$

for $n = 1, 3, 5$. At each order in the expansion, we then have to solve a set of two linear equations, which always have the same structure. We find as solutions

$$s_n = -\frac{q_n\chi_{11}^{QS} + m_n^S}{\chi_2^S} \tag{B4}$$

and

$$q_n = \frac{-m_n^B r\chi_2^S + m_n^Q\chi_2^S + m_n^S(r\chi_{11}^{BS} - \chi_{11}^{QS})}{(\chi_{11}^{QS})^2 - r\chi_{11}^{BS}\chi_{11}^{QS} + r\chi_2^S\chi_{11}^{BQ} - \chi_2^S\chi_2^Q}. \tag{B5}$$

At leading order one finds for the terms m_1^X,

$$m_1^B = \chi_2^B, \qquad m_1^Q = \chi_{11}^{BQ}, \qquad m_1^S = \chi_{11}^{BS}, \tag{B6}$$

and the contributions to the next-to-leading order expansion terms, m_3^X, are given by

$$\begin{aligned}
m_3^B =& \frac{1}{6}(3q_1^2s_1\chi_{121}^{BQS} + 3q_1s_1^2\chi_{112}^{BQS} + 6q_1s_1\chi_{211}^{BQS} + q_1^3\chi_{13}^{BQ} \\
&+ 3q_1^2\chi_{22}^{BQ} + 3q_1\chi_{31}^{BQ} + s_1^3\chi_{13}^{BS} + 3s_1^2\chi_{22}^{BS} + 3s_1\chi_{31}^{BS} + \chi_4^B) \\
m_3^Q =& \frac{1}{6}(3q_1^2s_1\chi_{31}^{QS} + 3q_1s_1^2\chi_{22}^{QS} + 6q_1s_1\chi_{121}^{BQS} + q_1^3\chi_4^Q \\
&+ 3q_1^2\chi_{13}^{BQ} + 3q_1\chi_{22}^{BQ} + s_1^3\chi_{13}^{QS} + 3s_1^2\chi_{112}^{BQS} \\
&+ 3s_1\chi_{211}^{BQS} + \chi_{31}^{BQ}) \\
m_3^S =& \frac{1}{6}(3q_1^2s_1\chi_{22}^{QS} + 3q_1s_1^2\chi_{13}^{QS} + 6q_1s_1\chi_{112}^{BQS} + q_1^3\chi_{31}^{QS} \\
&+ 3q_1^2\chi_{121}^{BQS} + 3q_1\chi_{211}^{BQS} + s_1^3\chi_4^S + 3s_1^2\chi_{13}^{BS} + 3s_1\chi_{22}^{BS} + \chi_{31}^{BS})
\end{aligned} \tag{B7}$$

Finally, the contributions to the next-to-next-to-leading order expansion terms, m_5^X, are given by

$$\begin{aligned}
m_5^B =& \frac{1}{120}(5q_1^4s_1\chi_{141}^{BQS} + 10q_1^3s_1^2\chi_{132}^{BQS} + 20q_1^3s_1\chi_{231}^{BQS} + 60q_1^2s_3\chi_{121}^{BQS} + 10q_1^2s_1^3\chi_{123}^{BQS} + 30q_1^2s_1^2\chi_{222}^{BQS} + 30q_1^2s_1\chi_{321}^{BQS} \\
&+ 120q_1s_1s_3\chi_{112}^{BQS} + 5q_1s_1^4\chi_{114}^{BQS} + 120q_3q_1s_1\chi_{121}^{BQS} + 120q_1s_3\chi_{211}^{BQS} + 20q_1s_1^3\chi_{213}^{BQS} + 30q_1s_1^2\chi_{312}^{BQS} \\
&+ 20q_1s_1\chi_{411}^{BQS} + 60q_3s_1^2\chi_{112}^{BQS} + 120q_3s_1\chi_{211}^{BQS} + q_1^5\chi_{15}^{BQ} + 5q_1^4\chi_{24}^{BQ} + 10q_1^3\chi_{33}^{BQ} + 60q_3q_1^2\chi_{13}^{BQ} \\
&+ 10q_1^2\chi_{42}^{BQ} + 120q_3q_1\chi_{22}^{BQ} + 5q_1\chi_{51}^{BQ} + 60q_3\chi_{31}^{BQ} + 60s_1^2s_3\chi_{13}^{BS} + s_1^5\chi_{15}^{BS} + 120s_1s_3\chi_{22}^{BS} \\
&+ 5s_1^4\chi_{24}^{BS} + 60s_3\chi_{31}^{BS} + 10s_1^3\chi_{33}^{BS} + 10s_1^2\chi_{42}^{BS} + 5s_1\chi_{51}^{BS} + \chi_6^B)
\end{aligned}$$

$$
\begin{aligned}
m_5^Q =& \frac{1}{120}(5q_1^4 s_1 \chi_{51}^{QS} + 10q_1^3 s_1^2 \chi_{42}^{QS} + 20q_1^3 s_1 \chi_{141}^{BQS} + 60q_1^2 s_3 \chi_{31}^{QS} + 10q_1^2 s_1^3 \chi_{33}^{QS} + 30q_1^2 s_1^2 \chi_{132}^{BQS} + 30q_1^2 s_1 \chi_{231}^{BQS} + 120q_1 s_1 s_3 \chi_{22}^{QS} \\
&+ 5q_1 s_1^4 \chi_{24}^{QS} + 120q_3 q_1 s_1 \chi_{31}^{QS} + 120q_1 s_3 \chi_{121}^{BQS} + 20q_1 s_1^3 \chi_{123}^{BQS} + 30q_1 s_1^2 \chi_{222}^{BQS} + 20q_1 s_1 \chi_{321}^{BQS} + 60q_3 s_1^2 \chi_{22}^{QS} + 120q_3 s_1 \chi_{121}^{BQS} \\
&+ q_1^5 \chi_6^Q + 5q_1^4 \chi_{15}^{BQ} + 10q_1^3 \chi_{24}^{BQ} + 60q_3 q_1^2 \chi_4^Q + 10q_1^2 \chi_{33}^{BQ} + 120q_3 q_1 \chi_{13}^{BQ} + 5q_1 \chi_{42}^{BQ} + 60q_3 \chi_{22}^{BQ} + 60s_1^2 s_3 \chi_{13}^{QS} + s_1^5 \chi_{15}^{QS} \\
&+ 120s_1 s_3 \chi_{112}^{BQS} + 5s_1^4 \chi_{114}^{BQS} + 60s_3 \chi_{211}^{BQS} + 10s_1^3 \chi_{213}^{BQS} + 10s_1^2 \chi_{312}^{BQS} + 5s_1 \chi_{411}^{BQS} + \chi_{51}^{BQ}) \\
m_5^S =& \frac{1}{120}(5q_1^4 s_1 \chi_{42}^{QS} + 10q_1^3 s_1^2 \chi_{33}^{QS} + 20q_1^3 s_1 \chi_{132}^{BQS} + 60q_1^2 s_3 \chi_{22}^{QS} + 10q_1^2 s_1^3 \chi_{24}^{QS} + 30q_1^2 s_1^2 \chi_{123}^{BQS} + 30q_1^2 s_1 \chi_{222}^{BQS} + 120q_1 s_1 s_3 \chi_{13}^{QS} \\
&+ 5q_1 s_1^4 \chi_{15}^{QS} + 120q_3 q_1 s_1 \chi_{22}^{QS} + 120q_1 s_3 \chi_{112}^{BQS} + 20q_1 s_1^3 \chi_{114}^{BQS} + 30q_1 s_1^2 \chi_{213}^{BQS} + 20q_1 s_1 \chi_{312}^{BQS} + 60q_3 s_1^2 \chi_{13}^{QS} + 120q_3 s_1 \chi_{112}^{BQS} \\
&+ q_1^5 \chi_{51}^{QS} + 5q_1^4 \chi_{141}^{BQS} + 10q_1^3 \chi_{231}^{BQS} + 60q_3 q_1^2 \chi_{31}^{QS} + 10q_1^2 \chi_{321}^{BQS} + 120q_3 q_1 \chi_{121}^{BQS} + 5q_1 \chi_{411}^{BQS} + 60q_3 \chi_{211}^{BQS} + 60s_1^2 s_3 \chi_4^S + s_1^5 \chi_6^S \\
&+ 120s_1 s_3 \chi_{13}^{BS} + 5s_1^4 \chi_{15}^{BS} + 60s_3 \chi_{22}^{BS} + 10s_1^3 \chi_{24}^{BS} + 10s_1^2 \chi_{33}^{BS} + 5s_1 \chi_{42}^{BS} + \chi_{51}^{BS}).
\end{aligned}
\tag{B8}
$$

In $(2+1)$-flavor QCD calculations the light (u, d) quark masses are taken to be degenerate. A consequence of this degeneracy is that not all generalized susceptibilities χ_{ijk}^{BQS} that enter the above expressions are independent. In a given order $n \equiv 2l \equiv i+j+k$ this results in a set of relations among the expansion coefficients. In general at order $n = 2l$, there are $l(l+1)$ constraints; i.e. for $l = 1$ this gives rise to two relations, [27]

$$
\begin{aligned}
0 &= \chi_2^B - 2\chi_{11}^{BQ} + \chi_{11}^{BS} \\
0 &= \chi_2^S - 2\chi_{11}^{QS} + \chi_{11}^{BS},
\end{aligned}
\tag{B9}
$$

for $l = 2$ there are six constraints,

$$
\begin{aligned}
0 &= \chi_4^B - 2\chi_{31}^{BQ} + \chi_{31}^{BS} \\
0 &= \chi_4^S - 2\chi_{13}^{QS} + \chi_{13}^{BS} \\
0 &= \chi_{22}^{BS} + \chi_{13}^{BS} - 2\chi_{112}^{BQS} \\
0 &= \chi_{31}^{BS} + \chi_{22}^{BS} - 2\chi_{211}^{BQS} \\
0 &= \chi_4^B - 6\chi_{31}^{BQ} + 12\chi_{22}^{BQ} - 8\chi_{13}^{BQ} + 3\chi_{31}^{BS} + 3\chi_{22}^{BS} + \chi_{13}^{BS} - 12\chi_{211}^{BQS} + 12\chi_{121}^{BQS} - 6\chi_{112}^{BQS} \\
0 &= \chi_4^S + \chi_{31}^{BS} + 3\chi_{22}^{BS} + 3\chi_{13}^{BS} - 8\chi_{31}^{QS} + 12\chi_{22}^{QS} - 6\chi_{13}^{QS} - 6\chi_{211}^{BQS} + 12\chi_{121}^{BQS} - 12\chi_{112}^{BQS},
\end{aligned}
\tag{B10}
$$

and for $l = 3$ there are 12 constraints,

$$
\begin{aligned}
&0 = \chi_6^B - 2\chi_{51}^{BQ} + \chi_{51}^{BS}, \quad 0 = \chi_{15}^{BS} - 2\chi_{15}^{QS} + \chi_6^S, \quad 0 = \chi_{42}^{BS} - 2\chi_{312}^{BQS} + \chi_{33}^{BS}, \quad 0 = \chi_{33}^{BS} - 2\chi_{213}^{BQS} + \chi_{24}^{BS}, \\
&0 = \chi_{51}^{BS} - 2\chi_{411}^{BQS} + \chi_{42}^{BS}, \quad 0 = \chi_{24}^{BS} - 2\chi_{114}^{BQS} + \chi_{15}^{BS}, \\
&0 = \chi_6^B - 6\chi_{51}^{BQ} + 12\chi_{42}^{BQ} - 8\chi_{33}^{BQ} + 3\chi_{51}^{BS} - 12\chi_{411}^{BQS} + 12\chi_{321}^{BQS} + 3\chi_{42}^{BS} - 6\chi_{312}^{BQS} + \chi_{33}^{BS}, \\
&0 = \chi_{33}^{BS} - 6\chi_{213}^{BQS} + 12\chi_{123}^{BQS} - 8\chi_{33}^{QS} + 3\chi_{24}^{BS} - 12\chi_{114}^{BQS} + 12\chi_{24}^{QS} + 3\chi_{15}^{BS} - 6\chi_{15}^{QS} + \chi_6^S, \\
&0 = \chi_{42}^{BS} - 6\chi_{312}^{BQS} + 12\chi_{222}^{BQS} - 8\chi_{132}^{BQS} + 3\chi_{33}^{BS} - 12\chi_{213}^{BQS} + 12\chi_{123}^{BQS} + 3\chi_{24}^{BS} - 6\chi_{114}^{BQS} + \chi_{15}^{BS}, \\
&0 = \chi_{51}^{BS} - 6\chi_{411}^{BQS} + 12\chi_{321}^{BQS} - 8\chi_{231}^{BQS} + 3\chi_{42}^{BS} - 12\chi_{312}^{BQS} + 12\chi_{222}^{BQS} + 3\chi_{33}^{BS} - 6\chi_{213}^{BQS} + \chi_{24}^{BS}, \\
&0 = \chi_6^B - 10\chi_{51}^{BQ} + 40\chi_{42}^{BQ} - 80\chi_{33}^{BQ} + 80\chi_{24}^{BQ} - 32\chi_{15}^{BQ} + 5\chi_{51}^{BS} - 40\chi_{411}^{BQS} + 120\chi_{321}^{BQS} - 160\chi_{231}^{BQS} + 80\chi_{141}^{BQS} + 10\chi_{42}^{BS} \\
&\quad - 60\chi_{312}^{BQS} + 120\chi_{222}^{BQS} - 80\chi_{132}^{BQS} + 10\chi_{33}^{BS} - 40\chi_{213}^{BQS} + 40\chi_{123}^{BQS} + 5\chi_{24}^{BS} - 10\chi_{114}^{BQS} + \chi_{15}^{BS}, \\
&0 = \chi_{51}^{BS} - 10\chi_{411}^{BQS} + 40\chi_{321}^{BQS} - 80\chi_{231}^{BQS} + 80\chi_{141}^{BQS} - 32\chi_{51}^{QS} + 5\chi_{42}^{BS} - 40\chi_{312}^{BQS} + 120\chi_{222}^{BQS} - 160\chi_{132}^{BQS} + 80\chi_{42}^{QS} + 10\chi_{33}^{BS} \\
&\quad - 60\chi_{213}^{BQS} + 120\chi_{123}^{BQS} - 80\chi_{33}^{QS} + 10\chi_{24}^{BS} - 40\chi_{114}^{BQS} + 40\chi_{24}^{QS} + 5\chi_{15}^{BS} - 10\chi_{15}^{QS} + \chi_6^S.
\end{aligned}
\tag{B11}
$$

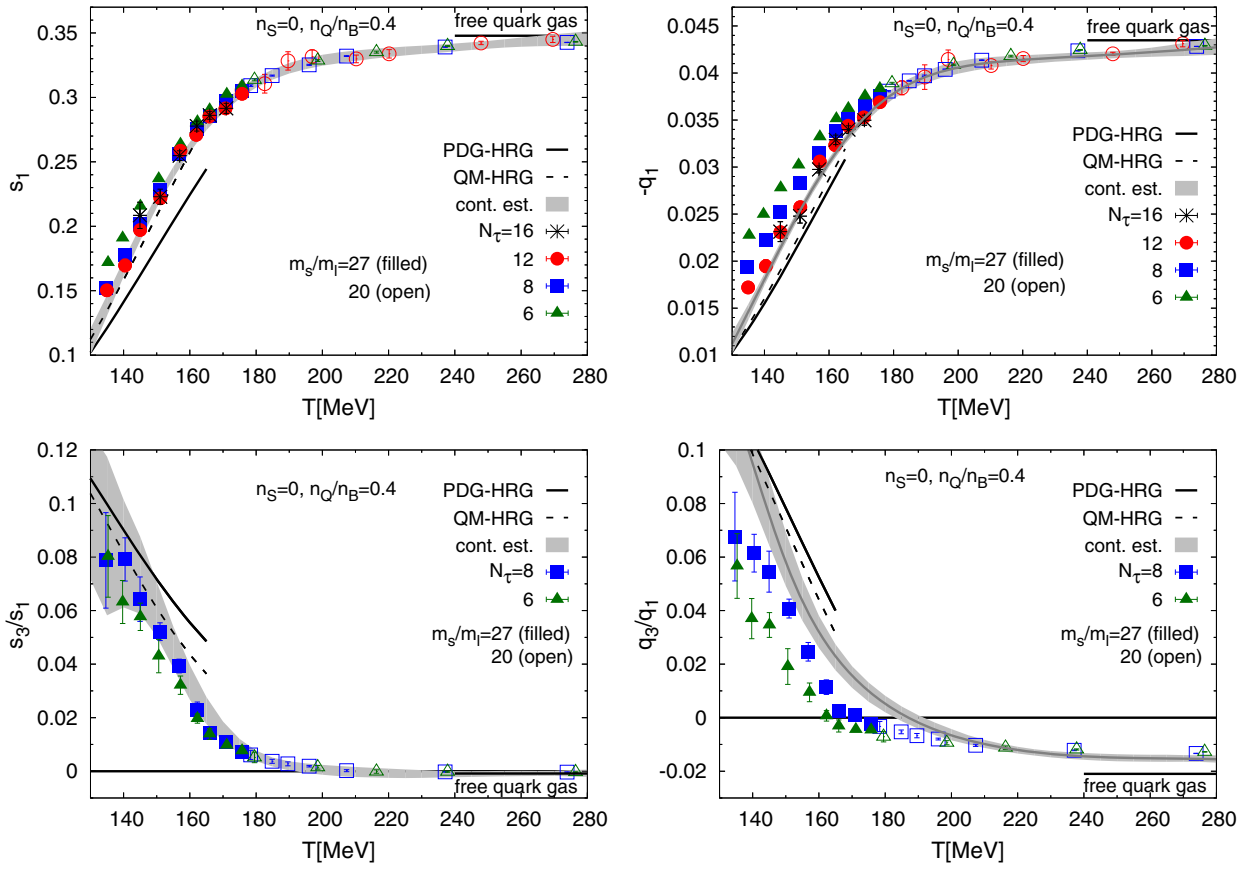

FIG. 17. The LO Taylor expansion coefficients s_1 (top left) and q_1 (top right) of the expansions of $\hat{\mu}_S$ and $\hat{\mu}_Q$ with respect to $\hat{\mu}_B$. The bottom set of figures show the ratios of NLO and LO expansion coefficients. The broad bands give the continuum extrapolated results. The curves inside these bands show results obtained with the interpolating curves introduced in Eq. (38). Also shown are the PDG-HRG and QM-HRG results (see text). The solid black lines labeled "free quark gas" denote the $T \to \infty$ noninteracting massless quark gas result.

Using these constraints it is tedious, but straightforward, to show that in the isospin symmetric case, $r = 1/2$, indeed all expansion coefficients for the electric charge chemical potential vanish; i.e. $\hat{\mu}_Q = 0$ to all orders in μ_B.

We show results for the LO expansion coefficients s_1 and q_1 and the ratios of the NLO and LO expansion coefficients, s_3/s_1 and q_3/q_1 in Fig. 17. As can be seen, the NLO coefficients are already negligible for $T \gtrsim 170$ MeV. The absolute value of the NNLO expansion coefficients s_5 and q_5 never is larger than 1% of the corresponding LO coefficients.

In Fig. 17, we also show results from hadron resonance gas (HRG) model calculations. The black curves are the predictions of the usual HRG model which consists of all the resonances listed in the Particle Data Group tables up to 2.5 GeV (PDG-HRG). The PDG-HRG results for s_1 are substantially smaller than the continuum-extrapolated lattice QCD results. It has been argued in [6] that this can be caused by contributions from additional, experimentally not yet observed, strange hadron resonances which are predicted in quark model calculations. A HRG model calculation based on such an extended resonance spectrum (QM-HRG) is also shown in Fig. 17. At finite values of the lattice cutoff we observe significant differences between lattice QCD calculations and both versions of the HRG models. This is, in particular, the case for the expansion coefficients of the electric charge chemical potentials. One thus may wonder whether these deviations can be understood in terms of taste violations in the staggered fermion formulation which result in a modification of the resonance spectrum and affect most strongly the light pseudoscalar (pion) sector.

APPENDIX C: THE COEFFCIENT κ_4^f OF LINES OF CONSTANT PHYSICS AT $\mathcal{O}(\mu_B^4)$

We present here results for the expansion coefficient κ_4^f of lines of constant physics defined in Eq. (43),

$$\kappa_4^f = \frac{\frac{1}{2}\frac{\partial^2 f(T,\mu_B)}{\partial T^2}|_{(T_0,0)}(\kappa_2^f)^2\frac{1}{T_0^2} - \frac{1}{2}\frac{\partial}{\partial T}\frac{\partial^2 f(T,\mu_B)}{\partial \mu_B^2}|_{(T_0,0)}\kappa_2^f\frac{1}{T_0} + \frac{1}{4!}\frac{\partial^4 f(T,\mu_B)}{\partial \mu_B^4}|_{(T_0,0)}}{\frac{\partial f(T,\mu_B)}{\partial T}|_{(T_0,0)}\frac{1}{T_0^3}}$$
$$= \frac{\frac{1}{2}T_0^2\frac{\partial^2 f_0(T)}{\partial T^2}|_{(T_0,0)}(\kappa_2^f)^2 - (T_0\frac{\partial f_2(T)}{\partial T}|_{(T_0,0)} - 2f_2(T_0))\kappa_2^f + f_4(T_0)}{T_0\frac{\partial f_0(T)}{\partial T}|_{(T_0,0)}}. \quad \text{(C1)}$$

The coefficients f_{2k} are defined by

$$f(T,\mu_B) = \sum_{k=0}^{\infty} f_{2k}\hat{\mu}_B^{2k}. \quad \text{(C2)}$$

In particular, we give explicit expressions for the case of constant pressure ($f \equiv P$), constant energy density ($f \equiv \epsilon$) and constant entropy density($f \equiv s$). For the pressure, we had the earlier expression [Eq. (15)]

$$\frac{P(T,\mu_B) - P(T,0)}{T^4} = \sum_{n=1}^{\infty} P_{2n}\hat{\mu}_B^{2n}. \quad \text{(C3)}$$

Comparing Eqs. (C3) and (C2) we have $f_0 = P(T,0) \equiv T^4 P_0$, $f_2 = T^4 P_2$ and $f_4 = T^4 P_4$. Thus,

$$\left.\frac{\partial f_0}{\partial T}\right|_{\mu_B} = \left.\frac{\partial P_0 T^4}{\partial T}\right|_{\mu_B} = T^3(TP_0' + 4P_0) \equiv s, \quad \text{(C4a)}$$

$$\left.\frac{\partial^2 f_0}{\partial T^2}\right|_{\mu_B} = \left.\frac{\partial^2 P_0 T^4}{\partial T^2}\right|_{\mu_B} = T^2(T^2P_0'' + 8TP_0' + 12P_0) \equiv \frac{C_V}{T}. \quad \text{(C4b)}$$

Here, s and C_V are the entropy density and specific heat per unit volume at vanishing chemical potential. Similarly,

$$\left.\frac{\partial f_2}{\partial T}\right|_{\mu_B} = \left.\frac{\partial P_2 T^4}{\partial T}\right|_{\mu_B} = T^3(TP_2' + 4P_2). \quad \text{(C5)}$$

Putting everything together we get, for the pressure

$$\kappa_4^P = \frac{1}{TP_0' + 4P_0}\left[P_4 - \kappa_2^P(TP_2' + 2P_2) + \frac{1}{2}(\kappa_2^P)^2(T^2P_0'' + 8TP_0' + 12P_0)\right]$$
$$= \frac{T^3}{s}\left[P_4(T) - \kappa_2^P\sigma_2(T) + \frac{1}{2}(\kappa_2^P)^2\frac{C_V}{T^3}\right], \quad \text{(C6)}$$

where σ_2 denotes the $\mathcal{O}(\hat{\mu}_B^2)$ expansion coefficient of the entropy density as introduced in Eq. (24).

Next, we consider κ_4^ϵ. Since the energy density is also of dimension four, we only need to replace P_{2n} with ϵ_{2n} in the first line of Eq. (C6). With this, we obtain

$$\kappa_4^\epsilon = \frac{1}{T\epsilon_0' + 4\epsilon_0}\left[\epsilon_4 - \kappa_2^\epsilon(T\epsilon_2' + 2\epsilon_2) + \frac{1}{2}(\kappa_2^\epsilon)^2(T^2\epsilon_0'' + 8T\epsilon_0' + 12\epsilon_0)\right]. \quad \text{(C7)}$$

Since $C_V \equiv (\partial\epsilon_0/\partial T)_{\mu_B}$, the above may be written as

$$\kappa_4^\epsilon = \frac{T^3}{C_V}\left[\epsilon_4 - \kappa_2^\epsilon(T\epsilon_2' + 2\epsilon_2) + \frac{1}{2}(\kappa_2^\epsilon)^2\frac{1}{T^2}\frac{\partial C_V}{\partial T}\right]. \quad \text{(C8)}$$

Finally, we consider κ_4^s. Since the entropy density is of dimension three, Eqs. (C4) become

$$\left.\frac{\partial(sT^3)}{\partial T}\right|_{\mu_B} = T^2(Ts' + 3s),$$
$$\left.\frac{\partial^2(sT^3)}{\partial T^2}\right|_{\mu_B} = T(T^2s'' + 6Ts' + 6s), \quad \text{(C9)}$$

and therefore,

$$\kappa_4^\sigma = \frac{1}{Ts' + 3s}\left[\sigma_4 - \kappa_2^\sigma(T\sigma_2' + \sigma_2) + \frac{1}{2}(\kappa_2^\sigma)^2(T^2s'' + 6Ts' + 6s)\right]. \quad \text{(C10)}$$

To zeroth order, the specific heat is also given by $C_V = (\partial(Ts)/\partial T)_{\mu_B}$. Thus,

$$\kappa_4^\sigma = \frac{T^3}{C_V}\left[\sigma_4 - \kappa_2^\sigma(T\sigma_2' + \sigma_2) + \frac{1}{2}(\kappa_2^\sigma)^2\frac{1}{T^2}\frac{\partial C_V}{\partial T}\right]. \quad \text{(C11)}$$

[1] J. Engels, F. Karsch, H. Satz, and I. Montvay, Phys. Lett. **101B**, 89 (1981).
[2] S. Borsanyi, Z. Fodor, C. Hoelbling, S. D. Katz, S. Krieg, and K. K. Szabo, Phys. Lett. B **730**, 99 (2014).
[3] A. Bazavov *et al.* (HotQCD Collaboration), Phys. Rev. D **90**, 094503 (2014).
[4] A. Bazavov, T. Bhattacharya, M. Cheng, C. DeTar, H. T. Ding, S. Gottlieb, R. Gupta, P. Hegde *et al.*, Phys. Rev. D **85**, 054503 (2012).
[5] A. Majumder and B. Muller, Phys. Rev. Lett. **105**, 252002 (2010).
[6] A. Bazavov, H.-T. Ding, P. Hegde, O. Kaczmarek, F. Karsch, E. Laermann, Y. Maezawa, S. Mukherjee *et al.*, Phys. Rev. Lett. **113**, 072001 (2014).
[7] R. V. Gavai and S. Gupta, Phys. Rev. D **64**, 074506 (2001).
[8] C. R. Allton, S. Ejiri, S. J. Hands, O. Kaczmarek, F. Karsch, E. Laermann, C. Schmidt, and L. Scorzato, Phys. Rev. D **66**, 074507 (2002).
[9] R. V. Gavai and S. Gupta, Phys. Rev. D **68**, 034506 (2003).
[10] C. R. Allton, S. Ejiri, S. J. Hands, O. Kaczmarek, F. Karsch, E. Laermann, and C. Schmidt, Phys. Rev. D **68**, 014507 (2003).
[11] C. R. Allton, M. Doring, S. Ejiri, S. J. Hands, O. Kaczmarek, F. Karsch, E. Laermann, and K. Redlich, Phys. Rev. D **71**, 054508 (2005).
[12] S. Ejiri, F. Karsch, E. Laermann, and C. Schmidt, Phys. Rev. D **73**, 054506 (2006).
[13] S. Borsanyi, G. Endrodi, Z. Fodor, S. D. Katz, S. Krieg, C. Ratti, and K. K. Szabo, J. High Energy Phys. 08 (2012) 053.
[14] J. Gunther, R. Bellwied, S. Borsanyi, Z. Fodor, S. D. Katz, A. Pasztor, and C. Ratti, arXiv:1607.02493.
[15] M. D'Elia, G. Gagliardi, and F. Sanfilippo, arXiv: 1611.08285.
[16] M. Asakawa and K. Yazaki, Nucl. Phys. **A504**, 668 (1989).
[17] M. A. Halasz, A. D. Jackson, R. E. Shrock, M. A. Stephanov, and J. J. M. Verbaarschot, Phys. Rev. D **58**, 096007 (1998).
[18] A. Vuorinen, Phys. Rev. D **68**, 054017 (2003).
[19] E. Follana, Q. Mason, C. Davies, K. Hornbostel, G. P. Lepage, J. Shigemitsu, H. Trottier, and K. Wong (HPQCD and UKQCD Collaborations), Phys. Rev. D **75** 054502 (2007).
[20] A. Bazavov *et al.* (HotQCD Collaboration), Phys. Rev. D **86** 034509 (2012).
[21] P. Hasenfratz and F. Karsch, Phys. Lett. **125B**, 308 (1983).
[22] R. V. Gavai and S. Sharma, Phys. Rev. D **85**, 054508 (2012).
[23] R. V. Gavai and S. Sharma, Phys. Lett. B **749**, 8 (2015).
[24] B. Friman, F. Karsch, K. Redlich, and V. Skokov, Eur. Phys. J. C **71**, 1694 (2011).
[25] C. Bonati, M. D'Elia, M. Mariti, M. Mesiti, F. Negro, and F. Sanfilippo, Phys. Rev. D **93**, 074504 (2016).
[26] A. Roberge and N. Weiss, Nucl. Phys. **B275**, 734 (1986).
[27] A. Bazavov, H. T. Ding, P. Hegde, O. Kaczmarek, F. Karsch, E. Laermann, S. Mukherjee, P. Petreczky *et al.*, Phys. Rev. Lett. **109**, 192302 (2012).
[28] R. Hagedorn and J. Rafelski, Phys. Lett. **97B**, 136 (1980).
[29] V. V. Dixit, F. Karsch, and H. Satz, Phys. Lett. **101B**, 412 (1981).
[30] A. Andronic, P. Braun-Munzinger, J. Stachel, and M. Winn, Phys. Lett. B **718**, 80 (2012).
[31] V. Vovchenko, M. I. Gorenstein, and H. Stoecker, arXiv: 1609.03975.
[32] J. Cleymans and K. Redlich, Phys. Rev. C **60**, 054908 (1999).
[33] J. Cleymans, H. Oeschler, K. Redlich, and S. Wheaton, Phys. Rev. C **73**, 034905 (2006).
[34] B. Tomasik and U. A. Wiedemann, Phys. Rev. C **68**, 034905 (2003).
[35] J. Cleymans, H. Oeschler, K. Redlich, and S. Wheaton (NA49 Collaboration), Phys. Lett. B **615**, 50 (2005).
[36] J. Rafelski and J. Letessier, J. Phys. G **36**, 064017 (2009).
[37] M. Petran and J. Rafelski, Phys. Rev. C **88**, 021901 (2013).
[38] J. Rafelski and M. Petran, Phys. Part. Nucl. **46**, 748 (2015).
[39] S. Das (STAR Collaboration), Eur. Phys. J. Web Conf. **90**, 08007 (2015).
[40] M. Floris, Nucl. Phys. **A931**, 103 (2014).
[41] F. Becattini, J. Steinheimer, R. Stock, and M. Bleicher, Phys. Lett. B **764**, 241 (2017).
[42] O. Kaczmarek, F. Karsch, E. Laermann, C. Miao, S. Mukherjee, P. Petreczky, C. Schmidt, W. Soeldner, and W. Unger, Phys. Rev. D **83**, 014504 (2011).
[43] G. Endrodi, Z. Fodor, S. D. Katz, and K. K. Szabo, J. High Energy Phys. 04 (2011) 001.
[44] C. Bonati, M. D'Elia, M. Mariti, M. Mesiti, F. Negro, and F. Sanfilippo, Phys. Rev. D **92**, 054503 (2015).
[45] R. Bellwied, S. Borsanyi, Z. Fodor, J. Günther, S. D. Katz, C. Ratti, and K. K. Szabo, Phys. Lett. B **751**, 559 (2015).
[46] P. Cea, L. Cosmai, and A. Papa, Phys. Rev. D **93**, 014507 (2016).
[47] R. V. Gavai and S. Gupta, Phys. Rev. D **71**, 114014 (2005).
[48] F. Karsch, B. J. Schaefer, M. Wagner, and J. Wambach, *Proc. Sci.*, LATTICE2011 (2011) 219.
[49] Z. Fodor and S. D. Katz, J. High Energy Phys. 04 (2004) 050.
[50] S. Datta, R. V. Gavai, and S. Gupta, arXiv:1612.06673.
[51] S. Datta, R. V. Gavai, and S. Gupta, *Proc. Sci.*, LATTICE20132014 (2014) 202.